

## Article

# Water, Salt, and Ion Transport and Its Response to Water-Saving Irrigation in the Hetao Irrigation District Based on the SWAT-Salt Model

Chang Ao<sup>1</sup>, Donglin Jiang<sup>2</sup>, Ryan T. Bailey<sup>3</sup>, Jianhua Dong<sup>1</sup>, Wenzhi Zeng<sup>1,4,\*</sup>  and Jiasheng Huang<sup>1</sup>

<sup>1</sup> State Key Laboratory of Water Resources Engineering and Management, Wuhan University, Wuhan 430072, China; aochang@whu.edu.cn (C.A.)

<sup>2</sup> Power China ZhongNan Engineering Corporation Limited, Changsha 410027, China

<sup>3</sup> Department of Civil and Environmental Engineering, Colorado State University, Fort Collins, CO 80523, USA

<sup>4</sup> College of Agricultural Science and Engineering, Hohai University, Nanjing 211100, China

\* Correspondence: zengwenzhi1989@hhu.edu.cn

**Abstract:** Soil salinization is one of the main hazards affecting the sustainable development of agriculture in the Hetao Irrigation District (HID) of Inner Mongolia. To grasp the water and salt transport patterns and spatial–temporal distribution characteristics of the HID at the regional scale, the improved Soil and Water Assessment Tool with a salinity module (SWAT-Salt) model was used to establish the distributed water and salt transport model for the watershed in this study. The results demonstrated that the modified model could more accurately represent the process of water and salt changes in the HID. The coefficient of determination ( $R^2$ ) in the simulation of streamflow and discharge salt loading was 0.83 and 0.86, respectively, and the Nash–Sutcliffe efficiency (NSE) was 0.80 and 0.74, respectively. Based on this, different hydrological processes (surface runoff, lateral flow, groundwater, soil seepage) as well as spatial–temporal distribution characteristics of water salinity in groundwater and soil were analyzed in the HID. Differences in groundwater and soil salinity in different land uses and soil types were also compared. Of these, surface runoff and lateral flow salt discharge loading are concentrated in the southwestern portion of the basin, while groundwater salt discharge loading is concentrated in the eastern as well as southwestern portions of the basin. The salt discharge loading from groundwater accounts for about 98.7% of the total salt discharge loading from all hydrological pathways and is the major contributing part of salt discharge from the irrigation area. Soil salinity increases gradually from west to east. Groundwater salinity (2946 mg/L) and soil water electrical conductivity (0.309 dS/m) were minimized in the cropland. Meanwhile, rational allocation of irrigation water can appropriately increase the amount of salt discharge loading. In conclusion, the model could provide a reference for the investigation of soil salinization and water–salt management measures in irrigation areas.



**Citation:** Ao, C.; Jiang, D.; Bailey, R.T.; Dong, J.; Zeng, W.; Huang, J. Water, Salt, and Ion Transport and Its Response to Water-Saving Irrigation in the Hetao Irrigation District Based on the SWAT-Salt Model. *Agronomy* **2024**, *14*, 953. <https://doi.org/10.3390/agronomy14050953>

Academic Editor: Yang Gao

Received: 6 April 2024

Revised: 27 April 2024

Accepted: 29 April 2024

Published: 2 May 2024

**Keywords:** SWAT-Salt; Hetao Irrigation District; water–salt transport; spatial–temporal distribution; salinity module



**Copyright:** © 2024 by the authors. Licensee MDPI, Basel, Switzerland. This article is an open access article distributed under the terms and conditions of the Creative Commons Attribution (CC BY) license (<https://creativecommons.org/licenses/by/4.0/>).

## 1. Introduction

Soil salinization can lead to reduced crop yields and seriously endanger the health of the soil environment. It is among the primary elements influencing the steady development of agricultural irrigation regions [1–3]. The topography of the Hetao Irrigation District (HID) is flat, and the drainage capacity is poor, which leads to an annual salt accumulation of about 1.5 million tons in the HID. In addition, transitional irrigation has led to a long-term high groundwater level in the HID. Soil salinization has been increasing year by year, seriously hampering the sustainable development of agricultural modernization in the HID [4–6].

Numerous academics have conducted pertinent research based on various spatial scales about the spatial–temporal distribution features of salt and water in the HID and the dynamic change law. At the field scale, field water and salt data were obtained by carrying out field experiments, combined with numerical modeling to analyze the water and salt transport patterns in the HID. Ramos et al. [7] modeled soil water–salt transport, boundary fluxes, and conductivity in the HID using a static groundwater table analyzer and HYDRUS-1D, which showed that soil salt accumulation was strongly related to irrigation and capillary fluxes. The findings showed a high correlation between irrigation and capillary flow and the formation of soil salt. Irrigation in autumn is essential for controlling soil salinity. Moreover, the best way to control salinity is to control the depth of saline groundwater. Using HYDRUS-2D, a model based on field experiments, Dou et al. [8] simulated the dynamic changes of soil moisture and salinity in the range of 0–100 cm using sunflowers in the HID as the research object. The HYDRUS-2D model was calibrated and validated in 2020 and 2021 using the measurements of soil salinity and moisture. It was found that the model simulation was better and the optimum drainage depth of 50 cm was finally determined for sunflowers. Lu et al. [9] utilized the simultaneous heat and water (SHAW) model to analyze the variations of soil hydrothermal salt transport in HID under different mulch cover treatments and autumn irrigation conditions throughout the year. It was discovered that the optimum mulching treatment for the Shahaoqu Experimental Station in HID, Inner Mongolia, was 0.9 kg/m<sup>2</sup> of straw mulch. To simulate the dynamics of soil water and salt in the saline wasteland of the HID, Yuan [10] employed the soil–water–atmosphere–plant (SWAP) model. It was determined that the soil water content showed a gradual rise, while the soil salt concentration exhibited a gradual decline throughout the autumn irrigation season. Saline barrens are essential for regulating the salt balance and managing the levels of salinity in the HID. They contribute to maintaining the dynamic equilibrium within the ecosystem. Mao et al. [11] proposed a loosely coupled SALTMOD model to simulate soil water salt and groundwater salt transport processes under combined well and canal irrigation. The study found a small amount of salt accumulation in the well-irrigated area’s root zone. The accumulation of salt mainly took place in the aquifer within the irrigation area that is served by both wells and canals. The model used in the above study has a good fit for simulating soil water and salt transport processes at the field scale. However, on the regional scale, the actual environment is more complex. It is susceptible to the superimposed influence of both man-made and natural factors, such as different land uses, soil types, agricultural cultivation management methods, topographic features, and meteorological conditions. The variability of water and salt transportation and spatial distribution in the HID is more significant. Therefore, these models have some constraints in studying water and salt transport at the regional scale.

The spatial–temporal distributions of groundwater and soil water salts are characterized by a certain degree of variability at the regional scale. In this regard, many scholars have carried out corresponding studies and research [12,13]. Chang et al. [5] employed the SaltMod model to simulate changes in cropland and saline wasteland caused by long-term salinization in the HID under different water management scenarios. They concluded that over the next 10 years, there would be an increase in irrigation water use of about 10–20% in the autumn and a reduction in soil salinity of about 1.06–10.92%. Hu et al. [14] combined several statistical methods to quantitatively analyze soil salinity and water content in the HID. The research showed that soil salinity increased with the decrease in groundwater depth in an exponential relationship. The soil particle size had an impact on the distribution pattern of salinity and moisture. Huang et al. [15] collected data on soil salinity and crop growth at the scale of the whole irrigation area combined with remote sensing inversion to resolve the spatial distribution differences of soil salinity and analyzed the impact of putting different salinity levels on crop planting, growth, and yield. The above methods can well predict the regional water and salt distribution, but the number and reliability of the samples are the key to determining the accuracy and precision of the prediction results. To quantitatively grasp the regional water and salt transport patterns, some scholars

have adopted the coupling of field-scale and regional-scale models to carry out related research. Hao et al. [16] coupled the HYDRUS-1D model with the erosion–productivity impact calculator (EPIC) crop growth module using distributed simulation in the irrigation domain of Jiefangzha in the HID as the study object. The coupled model was evaluated by the data of soil water salinity and crop growth, which well reflected the spatial variability problem of water salinity in the study area. Xu et al. [17] adopted a coupled model of SWAP and MODFLOW, which better reflected the groundwater flow process in the Yonglian test area of the HID and laid a good foundation for the solute transport process in the region. The Soil and Water Assessment Tool (SWAT) model has been widely used as a distributed hydrological model by scholars. Xiong et al. [18] developed a SWAT-AG (a modified SWAT for agricultural hydrological modeling) model, which can simulate the close interaction between soil water and shallow groundwater, taking into account the capillary rise effect. Tests were conducted in the HID, the result being that SWAT-AG performs well in simulating soil water and salt dynamics, groundwater depth fluctuations, plant growth, and water consumption and is significantly better than the original SWAT model. The SWAT-AG model was also used by Wang et al. [19] to investigate the effects of climate variability and human activities on water cycle changes in the HID. It was found that the large increase in evapotranspiration was mainly influenced by climatic conditions, while subsurface hydrological processes were mainly influenced by human activities, such as irrigation management. In addition, Liu et al. [20] introduced remote sensing images to calibrate the SWAT model in order to improve its runoff simulation accuracy in the HID. The results show that the coupled method improves the performance of the SWAT model by about 20% over the original SWAT model, which can effectively improve the simulation performance of the SWAT model. Coupled models can overcome the limitations of single models [21,22]. The water exchange problem of different hydrological processes can be solved by transferring variables between models. However, the coupled model has some limitations in predicting the dynamic changes of water and salt, and it also increases the difficulty of parameter rate determination and the validation of the coupled process.

For a long time, large water irrigation to wash away salts has been the main measure for soil salinization management in the HID [23,24]. Nevertheless, as the water-saving irrigation policy is consistently enforced, the intended volume of water taken from the Yellow River within the HID will decrease from 5 billion m<sup>3</sup> to approximately 4 billion m<sup>3</sup>, and the amount of drainage and salt discharge will be inevitably reduced so that the water–salt balance system in the region will be broken. In the case of a large amount of salt accumulation in the HID every year, the question of “where did the salt go” has not been fully studied [6]. Hence, for practical purposes in the field of irrigation, a comprehensive understanding of the long-term spatial–temporal distribution patterns of water and salt in the irrigation zone, along with the mechanisms of their transportation, is essential. Based on the improved SWAT-Salt model, the distributed water and salt transport model of the HID was established in this study. The model is used to analyze the spatial–temporal trends of drainage salinity, groundwater salinity, and soil water salinity for different hydrological processes over a long time series on a regional scale. It also analyzes the changes in water salinity for different land uses and soil types. Finally, scenario analyses are used to make appropriate recommendations for the development of irrigation districts. It is crucial for guiding the sustainable development of irrigation areas and ensuring the efficient allocation of water resources.

## 2. Materials and Methods

### 2.1. Study Area

In China, the HID is a major production base for grains and cash crops. It is situated in the Inner Mongolia Autonomous Region’s northwest region between 40°12′–41°20′ N and 106°10′–109°30′ E (Figure 1). This region has a flat topography, an average elevation of 1007–1050 m, and is high in the southwest and low in the northeast. The HID has an arid climate, with low rainfall and high evaporation, with a multi-year average rainfall

of 139–222 mm and a multi-year average evaporation of 1999–2346 mm [25]. The HID is mainly irrigated by the Yellow River water introduced from 1 main canal and 13 trunk canals and discharged into the Wuliangsu Sea from 1 main drainage canal and 12 trunk canals (Figure 1). The Yellow River irrigation water has an average mineralization of 597 mg/L, compared to 1873 mg/L for the drainage water. The HID is divided into five irrigation areas from west to east in terms of regional management: Yigan Irrigation Area, Jiefangzha Irrigation Area, Yongji Irrigation Area, Yichang Irrigation Area, and Ulat Irrigation Area. With an average of four to six irrigations per year, the annual irrigation pattern is split into three categories: autumn irrigation (July–September), summer irrigation (April–June), and autumn watering (October–November). With an average annual crop area of roughly 7.62 million mu, maize, wheat, and sunflower are the main crops grown in the HID [26].

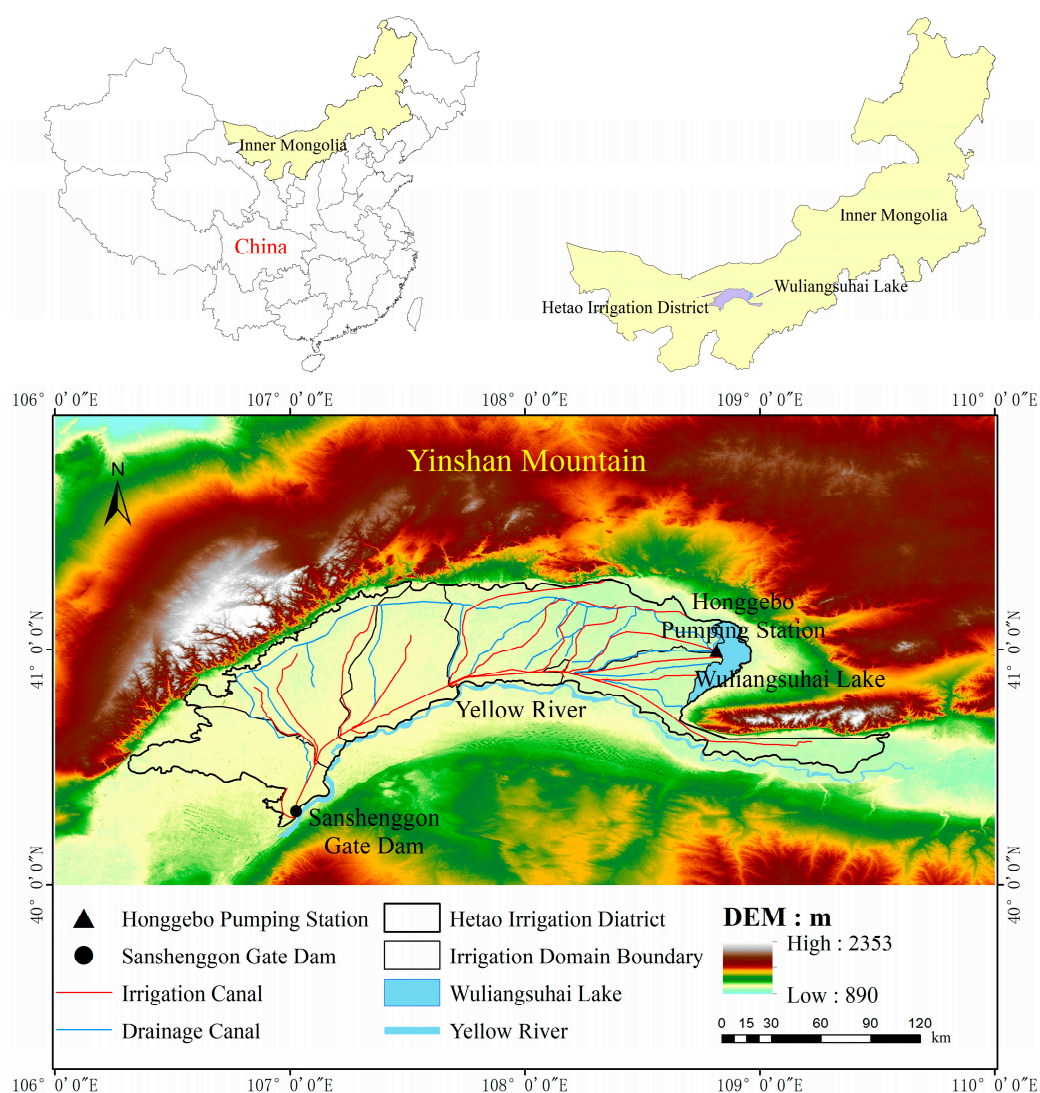


**Figure 1.** Location of the study area.

Anthropogenic accumulation soil and loose saline soil make up the majority of the soil types in the HID, making up over 90% of its total area. Saline soils in the HID are widely distributed, showing east-heavy, west-light, south-heavy, and north-light. The soil salt minerals are dominated by sulfate-salted soils, chloride-salted soils, and so on [27]. The average annual salt diversion in the HID from 1990 to 2013 was about  $280 \times 10^4$  t/year, and the salt discharge was about  $94.5 \times 10^4$  t/year. Groundwater sampling (1990–2007) from 116 observation wells in the basin of the whole HID was analyzed to obtain that

the groundwater contains eight ions, namely  $\text{SO}_4^{2-}$ ,  $\text{Ca}^{2+}$ ,  $\text{Cl}^-$ ,  $\text{Mg}^{2+}$ ,  $\text{K}^+$ ,  $\text{Na}^+$ ,  $\text{CO}_3^{2-}$ , and  $\text{HCO}_3^-$ . Among them,  $\text{SO}_4^{2-}$ ,  $\text{Na}^+$ ,  $\text{Cl}^-$ , and  $\text{HCO}_3^-$  are in large amounts, making up around 90% of the total quantity of salt ions. It has a multi-year average minimum mineralization of about 430 mg/L and an average maximum mineralization of about 39,600 mg/L.

## 2.2. SWAT-Salt Model

The SWAT model is an integrated hydrological model that is physically based and semi-distributed and operates in continuous time [28–30]. The SWAT model calculates precipitation, evapotranspiration, surface runoff, infiltration, loam flow, return flow, seepage, and submersible evaporation based on the water balance. The SWAT model can accurately simulate nutrient, pesticide, and sediment transport cycling processes in watersheds. It can be utilized to address issues such as agriculture and the health of water environments. However, its source code does not consider salt transport and transformation. However, salinity has a significant impact on crop growth, water quality, and soil environmental conditions in the majority of saline agricultural irrigation areas [31,32].

Bailey et al. [33] developed the SWAT-Salt model. The model simulates the movement of eight ions ( $\text{SO}_4^{2-}$ ,  $\text{Ca}^{2+}$ ,  $\text{Mg}^{2+}$ ,  $\text{Na}^+$ ,  $\text{K}^+$ ,  $\text{Cl}^-$ ,  $\text{CO}_3^{2-}$ , and  $\text{HCO}_3^-$ ) through surface runoff, lateral flow, soil infiltration, groundwater flow, and river flow. It is also possible to think about the five salt minerals' chemical reaction processes of precipitation–dissolution, complexation, and cation exchange ( $\text{CaCO}_3$ ,  $\text{MgCO}_3$ ,  $\text{CaSO}_4$ ,  $\text{MgSO}_4$ , and  $\text{NaCl}$ ). It is also simulated in each hydrological response unit (HRU). The mass balance equations for each salt ion at daily time steps in the HRU soil layer system are as follows:

$$S_{i,\text{soil},j} = S_{i,\text{soil},j-1} + S_{i,\text{irrig}} + S_{i,\text{soil,diss}} + S_{i,\text{revap}} - S_{i,\text{soil,precip}} - S_{i,\text{surf}} - S_{i,\text{lat}} - S_{i,\text{perc}} \quad (1)$$

where  $S_{i,\text{soil},j}$  and  $S_{i,\text{soil},j-1}$  denote the weight of the  $i$ -th ion in the soil on  $j$ -th and  $j-1$ -th day, respectively, kg/ha;  $S_{i,\text{irrig}}$  denotes the weight of the irrigation water, kg/ha;  $S_{i,\text{soil,diss}}$  denotes the weight of salt minerals dissolved as the salt ion in the soil layer, kg/ha;  $S_{i,\text{revap}}$  denotes the weight of the salt ion transported from the shallow aquifer to the soil layer, kg/ha;  $S_{i,\text{soil,precip}}$  denotes the weight of the salt ion precipitated as a salt mineral in the soil layer, kg/ha; and  $S_{i,\text{surf}}$ ,  $S_{i,\text{lat}}$ , and  $S_{i,\text{perc}}$  denote the weight of the  $i$ -th salt ion in surface runoff, lateral flow, and shallow aquifer, respectively, kg/ha. The above variables are unspecified to indicate the results for the  $i$ -th salt ion on the  $j$ -th day.

This study made use of the improved SWAT-Salt model. The main modifications were made to the point source salt module and the irrigation water salt module. The specific modifications and methods are available in Jiang et al. [34].

## 2.3. Data Input and Modeling

The SWAT-Salt model was created using the ArcSWAT interface, which is based on SWAT2012 [35]. The digital elevation model (DEM), groundwater and soil salinity concentrations, meteorological data, soil-type data, land use-type data, agricultural management data, and the mineralization of irrigation water from the Yellow River were among the input data (Table 1). The meteorological data were obtained from the precipitation (P), maximum and minimum temperature ( $T_{\text{max}}/T_{\text{min}}$ ), wind speed ( $U_2$ ), and relative humidity (RH) data from the national meteorological stations Linhe, Hangjin Houqi, Urat Zhongqi, and Baotou, and the solar radiation data were automatically generated using the CFSR World Weather Database R (<https://swat.tamu.edu/>) (accessed on 1 December 2021). Among them, Figure 2 shows the information of meteorological data in the study area.

**Table 1.** Input data sets for the SWAT model.

Data Type	Data Source	Data Description
DEM	Geospatial Data Cloud	Data resolution of 30 m
Land-use raster data	China Resource Satellite Application Research Center Gaofen-1 GF-1 data	Data resolution of 16 m, including different crop types, woodlands, wastelands, roads, waters and towns
Soil raster data	National Glacial Tundra Desert Science Data Center	The data scale is 1:1 million and includes the soil's physical and chemical properties
Meteorological data	National Weather Science Data Center and SWAT Official Website	Day-by-day meteorological data for 1990–2013. Rainfall, maximum and minimum temperatures, wind speed, and relative humidity data were monitored using national meteorological stations, and solar radiation was automatically generated using the CFSR global weather database on the SWAT website.
Ditch geo-mapping data	General Administration of the HID	Adoption of 2017 HID's geo-mapping information on dry canals and ditches
Agricultural management data	General Administration of the HID	Including monitoring data of hydrological stations in the HID from 1990 to 2013, diversion and drainage, annual crop planting area, etc.
Groundwater salinity data	General Administration of the HID	Includes monitoring data on salt ions from 116 observation wells in the HID on specific dates from 1990–2013

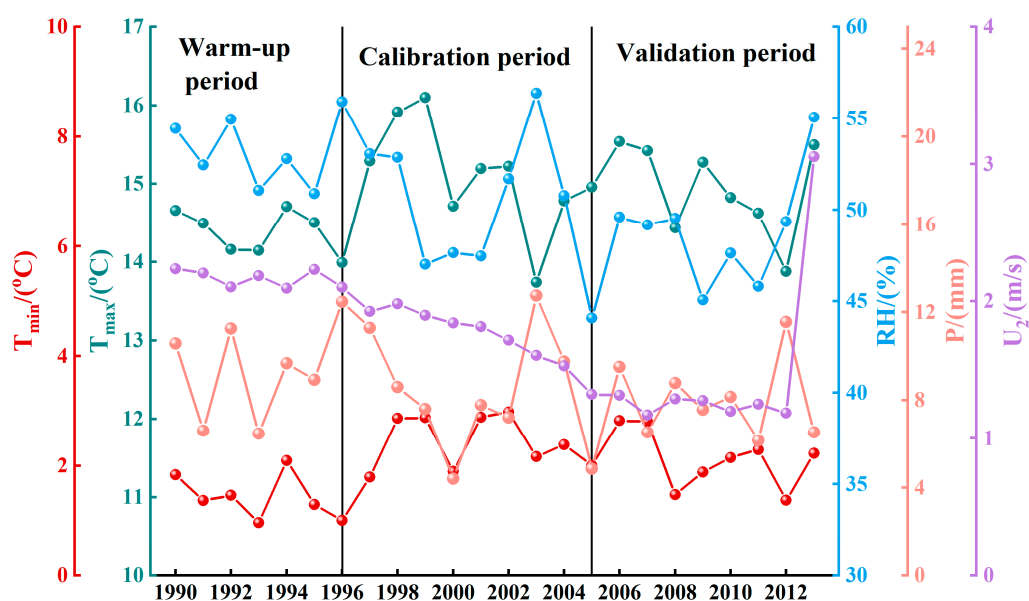


**Figure 2.** Information on meteorological data of HID.

The HID belongs to a typical plain irrigation area with artificial–natural double influence, and the complex artificial ditches in the irrigation area have changed the natural form of production and sinking. Therefore, the complete water system in the basin cannot be extracted based on the original DEM when dividing the river network, and the problem of spatial discretization becomes one of the difficulties in modeling distributed hydrological models [36]. The main soil types and land-use types are shown in Figure 3A,B. The study adopts the principle of “elevation incremental iterative algorithm” [37] and “burn in” [38] algorithm to process the DEM data so that the obtained DEM can better reflect the distribution of ditches and river networks in the HID. The sub-watersheds were manually modified

to make them consistent with the HID of the water management unit. The sub-watersheds and river networks were imported into SWAT through the pre-defined operation so that the watersheds were classified by the actual situation and management needs of the irrigation district. The original land-use raster data of the HID were reclassified using ArcGIS 10.5, and the different crop types were classified into four land-use types, namely, wheat, maize, sunflower, and other crops, and imported into SWAT. The thresholds for land-use type, soil type, and slope were established at 5%, 5%, and 5%, respectively, in the model, and a total of 62 sub-watersheds, 719 HRUs, and 4 watershed outlets were classified (Figure 3C).

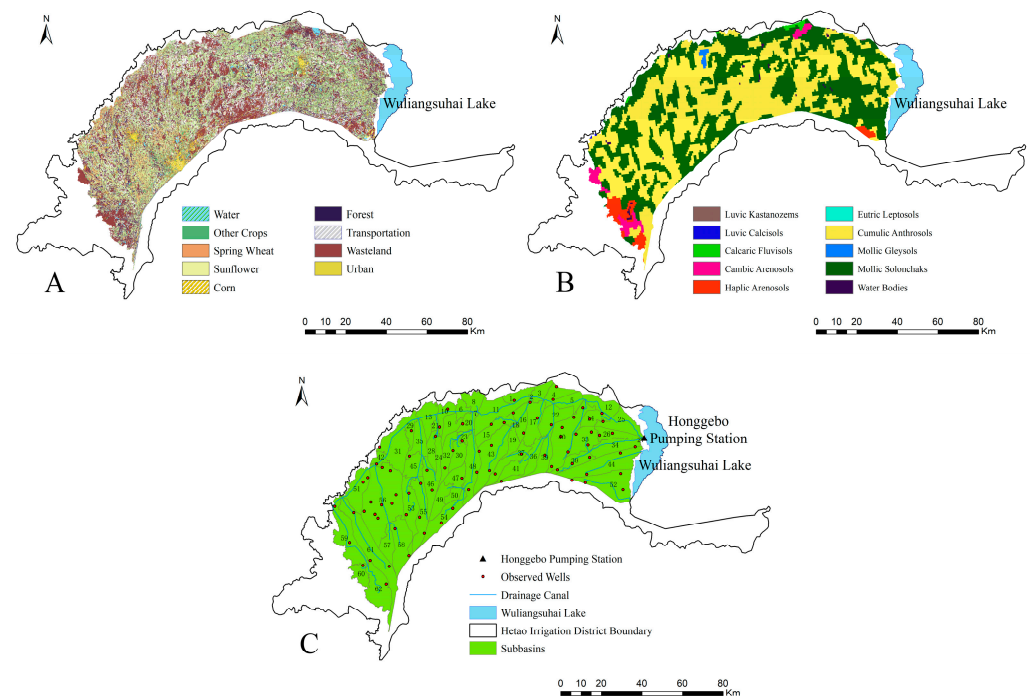


**Figure 3.** Land-use type (A), soil type (B), and sub-basin and observation well of study area (C).

The groundwater observation wells in the HID's initial monitoring period were used to determine the groundwater's initial salt ion concentration. The average of the concentrations of the eight salt ions in groundwater monitored in the corresponding observation wells in each sub-basin was assigned to the HRUs in the corresponding sub-basins. Groundwater observation wells are monitored on 16 January, 6 March, 26 May, 16 July, 16 September, 16 October, and 11 November each year. The Chinese soil dataset (v1.1) was used to determine the  $\text{CaCO}_3$  and  $\text{CaSO}_4$  content fractions in the soil layer [39] survey of the World Soil Database (HWSD) constructed by the Food and Agriculture Organization of the United Nations (FAO) and the International Institute for Applied Systems (IIASA), Vienna. Other mineral content fractions were initially set to 0. Each HRU's initial value for the salt ion concentration of soil water was set to be equal to that of groundwater. The difference between the two can be adjusted by setting a certain warm-up period [33]. The solubility product constants of salt minerals in the soil and aquifer were determined with reference to the relevant literature [33], where  $\text{CaCO}_3$ ,  $\text{MgCO}_3$ ,  $\text{CaSO}_4$ ,  $\text{MgSO}_4$ , and  $\text{NaCl}$  are  $3.07 \times 10^{-9}$ ,  $6.8 \times 10^{-6}$ ,  $4.9 \times 10^{-5}$ ,  $7.244 \times 10^{-3}$ , and 37.3, respectively. The conversion factor between total ion concentrations (TDS) (mg/L) in soil water and soil water electrical conductivity (EC) (dS/m) was set at 1562.7 ((mg/L)/(dS/m)) for the study.

## 2.4. Data Input and Modeling

### 2.4.1. Streamflow Calibration and Validation

In this study, the monthly average streamflow volume at the Red Ohb Hydrological Station at the outlet of the main drainage was obtained from the General Administration of

the HID. The 17 parameters that were chosen to be associated with changes in streamflow volume were calibrated and validated (Table 2) using the SUFI-2 algorithm in the SWAT Calibration and Uncertainty Programs (SWAT-CUP) program [40]. After determining the corresponding sensitivity parameters, a reasonable initial parameter range is selected. The Nash–Sutcliffe Efficiency (NSE) was used as the objective function after five iterations of 3000 simulations. The relevant parameters are adjusted after each iteration. The optimal parameter values are obtained by continuously reducing the error according to the objective function. The model is operational from 1990 to 2013, with the warm-up period being 1990–1995; the calibration period being 1996–2005; and the validation period being 2006–2013.

**Table 2.** Water parameters used for calibration and validation of the SWAT-Salt model.

Parameter	Definition	Ranges	Fitted Values	Rank
v_GWQMN.gw	Threshold depth of water level in the shallow aquifer for return base flow to occur (mm)	0.00~500.00	249.483	1
v_REVAPMN.gw	Threshold depth of water level in the shallow aquifer for revap to occur (mm)	0.00~500.00	399.51	2
v_GW_REVAP.gw	Groundwater revap coefficient	0.02~0.06	0.054	3
r_SOL_K().sol	Soil hydraulic conductivity (mm hr <sup>-1</sup> )	−0.80~0.80	0.094	4
r_SOL_AWC().sol	Available water capacity (mm mm <sup>-1</sup> )	−0.20~0.40	0.134	5
v_CH_K2.rte	Effective hydraulic conductivity of channel (mm h <sup>-1</sup> )	0.00~150.00	30.018	6
v_ALPHA_BNK.rte	Baseflow alpha factor of bank storage	0.00~1.00	0.876	7
v_ESCO.hru	Soil evaporation compensation factor	0.50~1.00	0.579	8
v_GW_DELAY.gw	Delay time for aquifer recharge (days)	0.00~40.00	17.422	9
v_OV_N.hru	Manning's n value for overland flow	0.01~0.35	0.256	10
v_EPCO.hru	Plant evaporation compensation factor	0.00~1.00	0.248	11
v_CH_N2.rte	Manning's n value for the main channel	0.00~0.30	0.091	12
r_CN2.mgt	SCS runoff curve number for Moisture condition II	−0.20~0.20	−00.094	13
v_RCHRG_DP.gw	Deep aquifer percolation fraction	0.00~0.20	0.193	14
v_ALPHA_BF.gw	Baseflow recession constant (days)	0.00~1.00	0.313	15
v_SFTMP.bsn	Snowfall temperature (°C)	−3.00~3.00	0.25	16
r_SOL_BD().sol	Moist bulk density (g cm <sup>-3</sup> )	−0.30~0.30	0.19	17

Note: v parameter value means substitute into realizing value or absolute change; r parameter value means multiplied by a value (1 + a given value) or relative change.

#### 2.4.2. Salinity Parameter Calibration and Validation

Salt ions in groundwater in the study area contain mainly Na<sup>+</sup>, Cl<sup>−</sup>, SO<sub>4</sub><sup>2−</sup>, and HCO<sub>3</sub><sup>−</sup>, with smaller proportions of Ca<sup>2+</sup>, Mg<sup>2+</sup>, K<sup>+</sup>, and CO<sub>3</sub><sup>2−</sup>. The HWSI investigated the content of CaCO<sub>3</sub> and CaSO<sub>4</sub> in each soil but did not record the content of NaCl. Therefore, the NaCl content is a large uncertainty and will influence the variation of Na<sup>+</sup> and Cl<sup>−</sup> concentrations in groundwater and soil water in the region. The NSE is used as the objective function to adjust the content of NaCl. Therefore, the NaCl initial content fraction corresponds to the soil type of Mollic Solonchaks (SCm) in the soil layer system and aquifer system of the HRU. Manual calibration was performed to alter the parameters for the salt simulation to calculate the correct magnitude of change in the monthly salt discharge loading at the basin outlet and the concentration of salt ions in the groundwater. The initial NaCl content fraction for SCm was adjusted from 0 to 0.063.

#### 2.4.3. Evaluation Indicators

The model results were evaluated using the coefficient of determination (R<sup>2</sup>), the NSE, and the percent bias (PBIAS) [41,42]. The model's correlation is better the closer the R<sup>2</sup> is to 1. Usually, R<sup>2</sup> > 0.5 is considered acceptable. The NSE value is a number between −∞ and 1, where a higher number indicates a better model. Positive values represent simulated

underestimation bias, while negative values represent simulated overestimation bias. A value of 0 is considered optimal.

$$R^2 = \left( \frac{\sum_{i=1}^n (Q_{obs,i} - \bar{Q}_{obs})(Q_{sim,i} - \bar{Q}_{sim})}{\sqrt{\sum_{i=1}^n (Q_{obs,i} - \bar{Q}_{obs})^2} \sqrt{\sum_{i=1}^n (Q_{sim,i} - \bar{Q}_{sim})^2}} \right)^2 \quad (2)$$

$$NSE = 1 - \frac{\sum_{i=1}^n (Q_{obs,i} - Q_{sim,i})^2}{\sum_{i=1}^n (Q_{obs,i} - \bar{Q}_{obs})^2} \quad (3)$$

$$PBIAS = \frac{\sum_{i=1}^n (Q_{obs,i} - Q_{sim,i})}{\sum_{i=1}^n (Q_{obs,i})} \times 100\% \quad (4)$$

where  $n$  represents the number of data points;  $i$  represents the time step;  $Q_{obs,i}$  and  $Q_{sim,i}$  represent the observed and simulated value, respectively, ( $m^3/s$ ); and  $\bar{Q}_{obs}$  and  $\bar{Q}_{sim}$  represent the observed and simulated value's arithmetic mean, respectively, ( $m^3/s$ ).

### 2.5. Scenario Setting for Water-Saving Irrigation

Following the adoption of the HID's directive water conservation policy, less water diversion will result in less irrigation water being used for fall watering and crop reproduction. In contrast, the irrigation district uses a significant portion of its annual water diversion—roughly 35–40%—for fall watering. Therefore, it is possible to analyze different water savings in irrigation districts during the reproductive and fall watering periods at the watershed scale by setting up different scenarios with three major and six minor categories (Table 3). The years 2008–2013 were used as the scenario simulation period. It was assumed that the input conditions, such as the existing crop cropping structure and irrigation water utilization coefficient, remain unchanged, and the meteorological data and irrigation water salinity concentration were input according to the scenario simulation period. The summer and fall irrigation volumes and the fall watering volume were set according to the actual irrigation volume of the year after reducing the corresponding proportion.

**Table 3.** Settings for different irrigation volume reduction ratio scenarios.

Scenarios		Total Irrigation Percentage of Reduction	Fertility Irrigation Percentage of Reduction	Irrigation Volume during Fall Watering Percentage of Reduction
Scenario 1	Scenario 1.1	0.05	0.05	0.05
	Scenario 1.2		0.00	0.10
Scenario 2	Scenario 2.1	0.10	0.10	0.10
	Scenario 2.2		0.05	0.20
Scenario 3	Scenario 3.1	0.15	0.15	0.15
	Scenario 3.2		0.10	0.25

## 3. Results

### 3.1. Calibration and Validation

#### 3.1.1. Streamflow

After repeatedly adjusting the range of values of runoff-sensitive parameters, the model was best fitted to the validation period.  $R^2$ , NSE, and PBIAS for the streamflow during the calibration period were 0.81, 0.80, and 1.2%, respectively; during the validation

period, these values were 0.83, 0.81, and 5.3%, respectively. The accuracy of the validation period simulations was slightly lower than that of the calibration period, but the simulation was better in both periods. According to the evaluation criteria of the relevant indicators, the model fitting accuracy is very good, which is in line with the simulation process of the change of monthly streamflow of the total drainage of the HID. The measured average monthly streamflow for the calibration period was 14.14 m<sup>3</sup>/s, whereas the simulated average monthly streamflow was 13.97 m<sup>3</sup>/s. Values of 14.77 m<sup>3</sup>/s for the simulated streamflow and 15.59 m<sup>3</sup>/s for the measured streamflow represented the average monthly streamflow during the validation period. Water balance is the driving force of all hydrological material cycling processes in the watershed. Table 4 and Figure 4 display the results of the calibration and validation.

**Table 4.** Monthly runoff calibration and verification results.

Period	R <sup>2</sup>	NSE	PBIAS	Average Monthly Water Volume (m <sup>3</sup> /s)	
				Observed Value	Simulated Value
Calibration	0.81	0.80	1.2%	14.14	13.97
Validation	0.83	0.81	5.3%	15.59	14.77

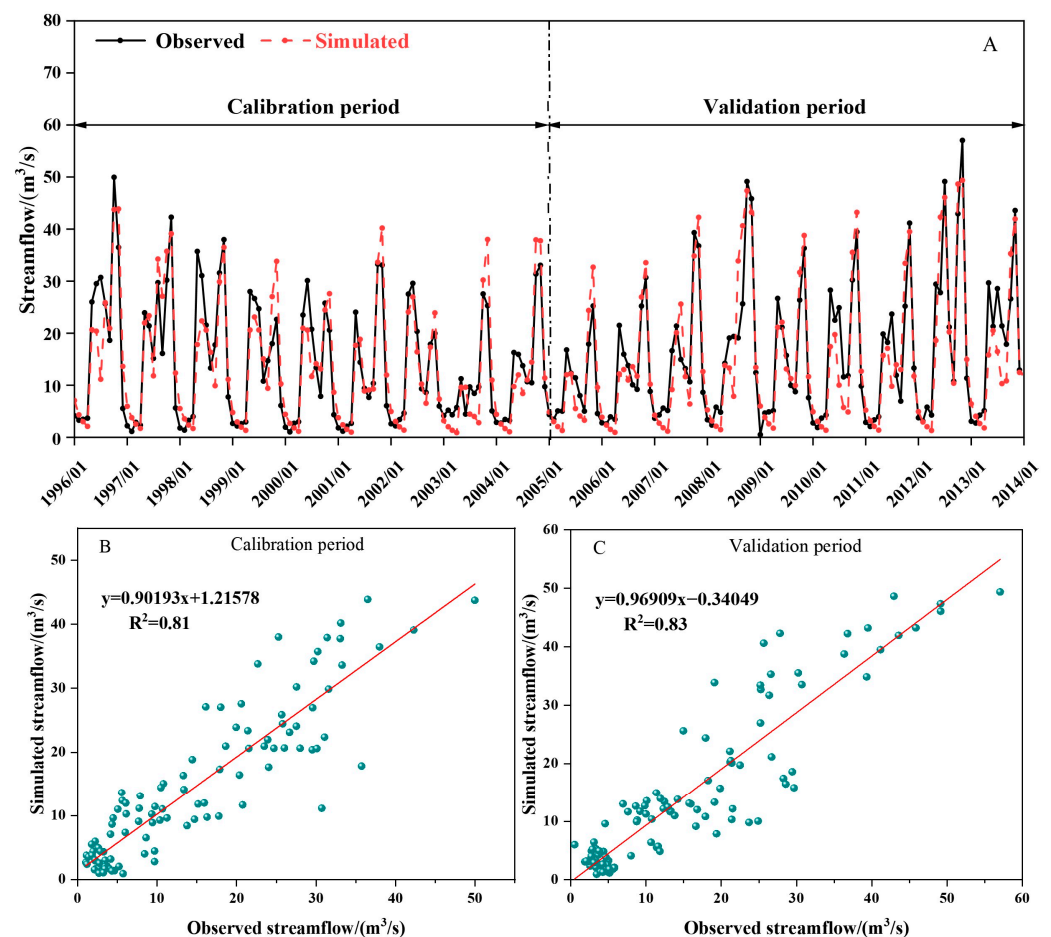


**Figure 4.** Monthly dynamics of simulated and observed runoff (A) in the outlet of the study area and scatter plots for the calibration (B) and validation (C) periods.

### 3.1.2. Total Salt Loading

Manual calibration was used to modify the solubility product constant and the percentage of original salt minerals in the aquifer and soil. The rates were calibrated and validated by comparing the measured monthly salt discharge monitored at the outlet section of the

watershed at the Hong Ohb station with the simulated values of the model. Evaluation metrics for the monthly salt loadings during the calibration period were an  $R^2$  of 0.89, NSE of 0.84, and PBIAS of 4.2%; for the monthly salt loadings during the validation period, the metrics were an  $R^2$  of 0.86, NSE of 0.74, and PBIAS of 3.7%. It was still better in both periods. During the validation period, the average monthly measured and simulated salt loading was  $9.15 \times 10^7$  kg and  $8.81 \times 10^7$  kg, respectively. Furthermore, the simulation results show that the model underestimates the annual salt discharge from December to April. According to the evaluation criteria of relevant indicators, the model simulation accuracy is good, and it can reflect the simulation process of the change in monthly salt discharge volume of the total drainage trunk in the HID. Table 5 and Figure 5 display the results of the calibration and validation.

**Table 5.** Monthly total salt discharge loading calibration and verification results.

Period	$R^2$	NSE	PBIAS	Monthly Salt Discharge Loading ( $10^7$ kg/mon)	
				Observed Value	Simulated Value
Calibration	0.89	0.84	4.2%	7.52	7.21
Validation	0.86	0.74	3.7%	9.15	8.81

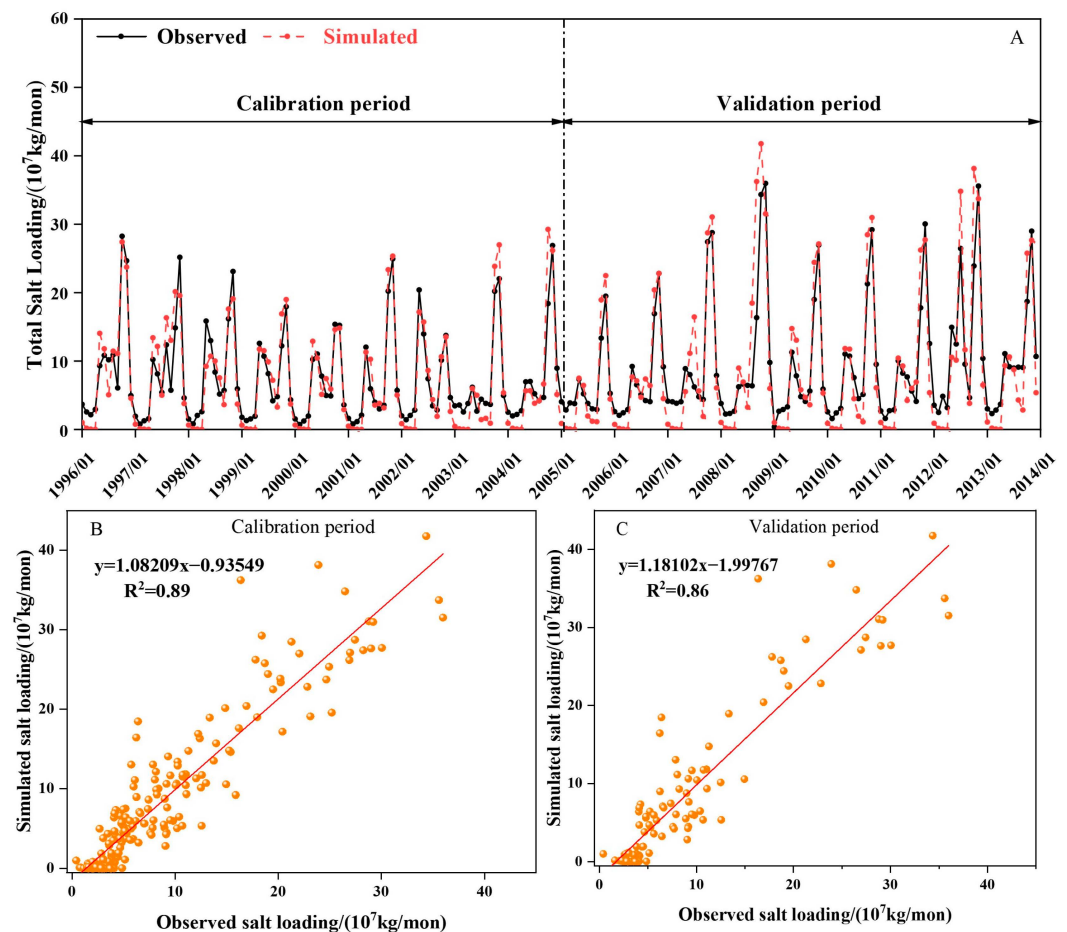


**Figure 5.** Inter-monthly dynamics of simulated and observed values of export salt loadings (A) in the study area and scatter plots for the calibration (B) and validation (C) periods.

### 3.1.3. SWAT-Salt Model before and after Improvement

The annual salt loading at the basin outlet before and after the model was modified is compared in Figure 6. The average annual salt discharge loading before and after modification of the model was  $2.61 \times 10^8$  kg/year and  $9.61 \times 10^8$  kg/year, respectively.

Nonetheless, the average yearly salt loading that has been observed is  $10.00 \times 10^8$  kg. It shows that the modification of the irrigation water salinity module can more accurately reflect the salt discharge situation in the HID. Consequently, following the modification of the irrigation water salt module, the trends of monthly streamflow change and monthly salt discharge loading change are essentially consistent with the observed trends. Moreover, the corresponding evaluation indexes are higher and better correlated. As a result, the HID's water and salt transport change process can be more clearly seen using the improved SWAT-Salt model. In summary, the distributed SWAT-Salt water and salt transport model established in this study for arid and semi-arid agricultural irrigation areas represented by the HID has good applicability. Therefore, the model is an effective research tool for analyzing the changing law of water and salt transport at the regional scale, which provides an important basis for improving the salinity problem in agricultural irrigation areas.

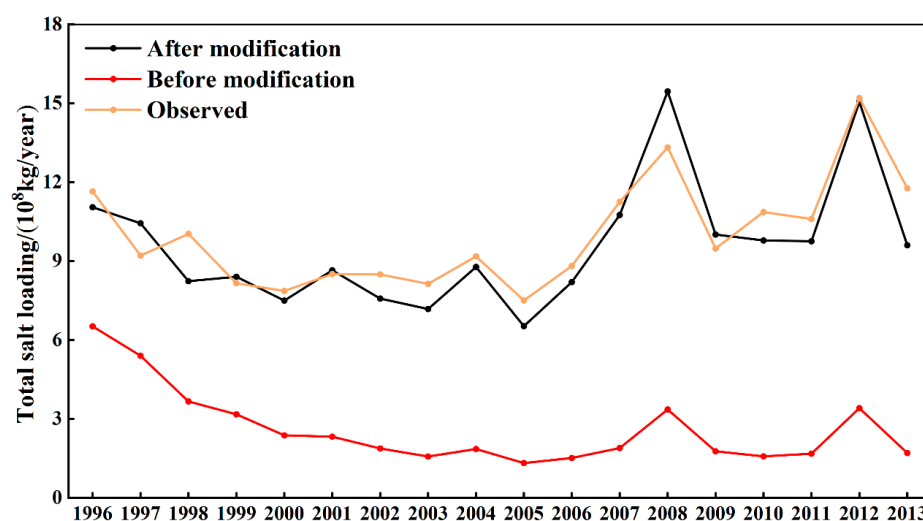


Figure 6. Comparison between before and after model improvement.

### 3.2. Changes in Drainage and Salt Discharge

Figure 7 shows the time-dependent process of eight ion concentrations and total ion concentrations (TDS) in the watershed outlet from 1996 to 2013. The cations in the ionic composition of drainage salts in the watershed outlet are mainly  $\text{Na}^+$ , and the anions in the composition are mainly  $\text{SO}_4^{2-}$ ,  $\text{Cl}^-$ , and  $\text{HCO}_3^-$ . The results are similar to the findings of other scholars. However, the concentrations of  $\text{Na}^+$  and  $\text{Cl}^-$  are underestimated in the ionic content [43–45], which may be related to the fact that the fraction of  $\text{NaCl}$  content was not recorded in the soil data survey. In addition, as can be seen in Figure 7C,E,H, the concentrations of  $\text{Mg}^{2+}$ ,  $\text{K}^+$ , and  $\text{HCO}_3^-$  show an increasing trend from year to year. The fluctuations in the concentrations of  $\text{SO}_4^{2-}$ ,  $\text{Ca}^{2+}$ , and  $\text{CO}_3^{2-}$  from year to year are relatively small, whereas the fluctuations in the concentrations of  $\text{Na}^+$  and  $\text{Cl}^-$  from year to year are relatively large. This may be because the solubility products of  $\text{CaCO}_3$  and  $\text{CaSO}_4$  are relatively small and the concentration of ions produced by dissolution fluctuates less. However, the solubility product constant of  $\text{NaCl}$  is relatively large, and the concentration of ions produced by dissolution fluctuates more.

By combining Figure 4, Figure 5, and Figure 7, it is possible to observe that the drainage and salt discharge loads in the HID vary year-round in two distinct peaks; one occurs during the crop fertility period, while the other occurs during the autumn watering period. It is caused by irrigation and rainfall during the fertile period as well as extensive irrigation to leach soil salts during the autumn watering period. It makes the total drainage and total salt discharge increase dramatically. The amounts of salt discharged during the reproductive period and the autumn watering period make up approximately 35.8% and 55.4% of the total annual salt discharge, respectively. Therefore, the irrigation salt washing

measures during the autumn watering period play a key role in the process of salt discharge and salt suppression in the HID.

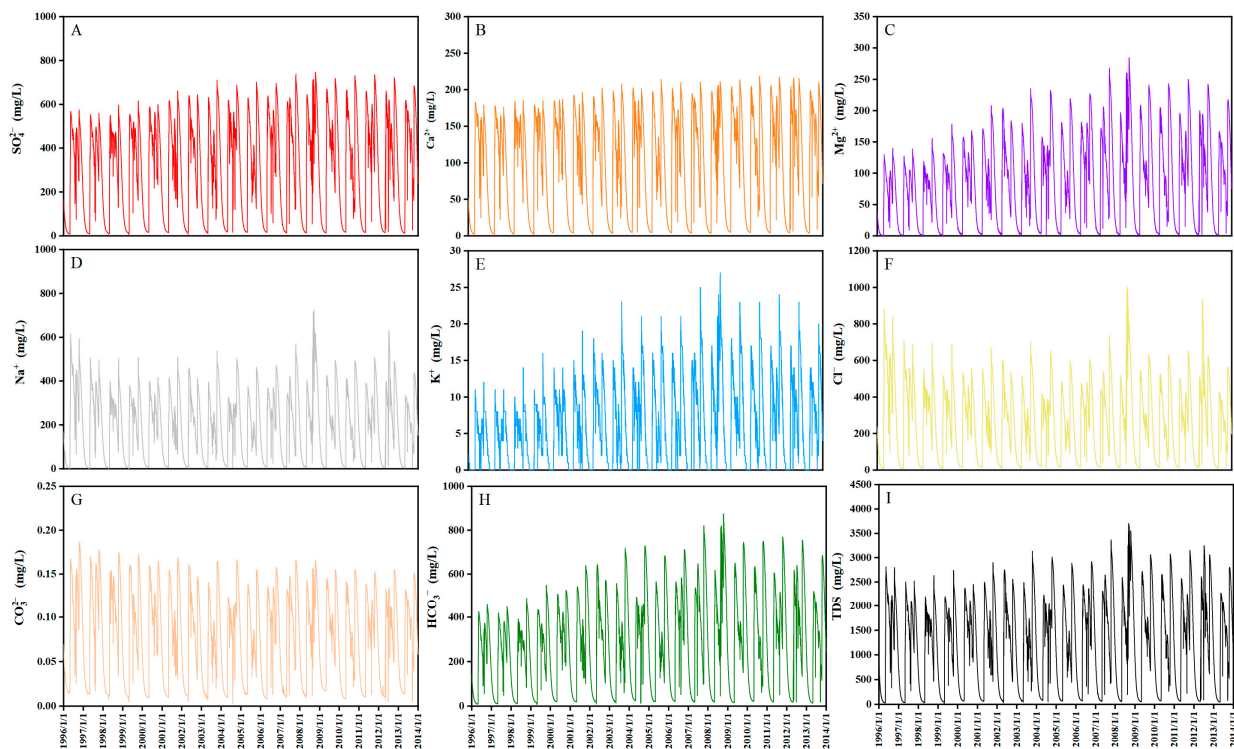


**Figure 7.** Changes in the concentration of eight ions ( $\text{SO}_4^{2-}$  (A),  $\text{Ca}^{2+}$  (B),  $\text{Mg}^{2+}$  (C),  $\text{Na}^+$  (D),  $\text{K}^+$  (E),  $\text{Cl}^-$  (F),  $\text{CO}_3^{2-}$  (G),  $\text{HCO}_3^-$  (H)) and TDS (I) at the outlet of the basin from 1996 to 2013.

### 3.3. Spatial–Temporal Variations of Water Salinity in Different Hydrological Processes

The intra-annual variation in salt loading is comparable to the variation in runoff. The three primary components of the hydrological runoff composition of the HID are groundwater runoff, soil lateral flow, and surface runoff. While the topography of the HID is relatively flat, surface runoff and soil lateral flow are relatively small. Drainage and salt drainage occur mainly through groundwater processes. Table 6 and Figure 8A indicate the annual contribution of salt discharge from different hydrological processes. Based on the findings of the statistical analysis of the model output, from 1996 to 2013, the annual average total salt production loading (surface runoff salt discharge loading + lateral flow salt discharge loading + groundwater salt discharge loading) was about 1509.4 kg/ha. Among them, the salt production from groundwater is the main contributing part of the total salt production, accounting for about 98.8% or so. Lateral flow and surface runoff contribute less. This highlights the fact that groundwater discharge plays a key role in salt removal from the HID. Figure 8B represents the annual variation of salt loading introduced through irrigation water and salt loading infiltrated. The average annual salt loading from irrigation water is 1.28 million tons, and the salt loading from soil leakage into the aquifer is 1.43 million tons. The results show that the main reason for the salt infiltration of the soil profile into the aquifer is the salt introduced by irrigation water. Moreover, the rest of the salt loading comes from the dissolution of saline minerals that are converted into salt ions in the groundwater by the dissolution chemical reaction. The variations in salt loading in the aquifer and soil layer over time are depicted in Figure 8C,D. The results showed that before 2007, the salt loading in the soil layer and aquifer in the HID showed an increasing trend year by year. The aquifer's salt loading remained constant after 2007, but the HID's soil layer salt loading trended lower after that year. This is due to the large amount of salt diversion in the HID before 2007. However, the overall drainage engineering measures were relatively weak, resulting in a small total salt discharge from the HID and

a gradual accumulation of salt in the soil layer and aquifer. Nevertheless, after 2007, as the drainage project improved bit by bit, the salinity of the soil layer dropped, and the salt discharge from the HID improved. Overall, the HID draws a large amount of salt each year. However, irrigation and precipitation leaching carry soil salts into groundwater. To prevent an increase in soil salinization in the HID, the drainage project’s improvement hastened the salt discharge in the HID.

**Table 6.** Salt loading of each hydrological path.

Year	Surface Runoff Salt Discharge (kg/ha)	Lateral Flow Salt Discharge (kg/ha)	Groundwater Salt Discharge (kg/ha)	Total Salt Production (kg/ha)
1996	0.013	14.19	1748.49	1762.70
1997	1.085	16.25	1620.95	1638.28
1998	0.009	15.73	1305.12	1320.86
1999	0.008	18.55	1337.59	1356.15
2000	0.015	18.31	1183.51	1201.84
2001	0.003	19.05	1364.44	1383.49
2002	0.025	18.73	1182.76	1201.51
2003	0.003	15.60	1143.41	1159.02
2004	0.008	17.33	1331.27	1348.61
2005	0.001	14.86	1010.92	1025.79
2006	0.004	16.11	1185.68	1201.80
2007	0.013	17.44	1629.74	1647.19
2008	0.017	20.87	2455.26	2476.15
2009	0.002	20.43	1564.30	1584.73
2010	0.011	17.10	1514.52	1531.63
2011	0.005	17.04	1524.30	1541.34
2012	0.036	18.25	2267.00	2285.29
2013	0.007	16.81	1485.36	1502.17

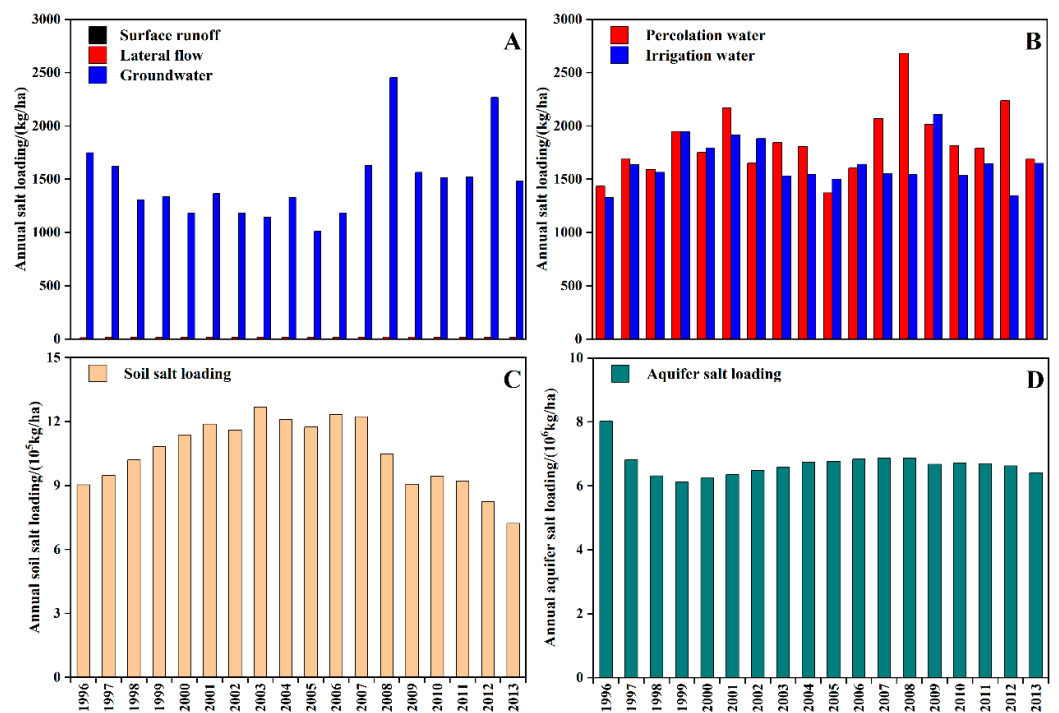


**Figure 8.** From 1996 to 2013, the salt discharge loading of each hydrological path (A), salt loading from irrigation water and soil percolation (B), soil salt loading (C), and aquifer salt loading (D).

The HID brings in a large amount of salt every year by diverting Yellow River irrigation. The quantity of salt decreases as less water is diverted from the Yellow River. Accordingly, the quantity of salt discharge will be decreased, as will the quantity of irrigation water used for fall watering and during the reproductive season. Conversely, as more water is diverted from the Yellow River, more water will be needed for irrigation during the reproductive season and for fall watering. This will also increase salt production and salt discharge. Consequently, the proper distribution of irrigation during the reproductive period and autumn watering is essential for the crop's normal growth and for washing away salt and suppressing it.

The study area's spatial distribution pattern of water and salt in the HID between 1996 and 2013 was examined using SWAT-Salt simulation, which models various hydrological processes and salt loadings in the aquifer and soil layer of each HID sub-basin. The results indicated that the spatial distribution of salt loading in each sub-basin had large variability. The average yearly salt loading that each sub-basin of the HID discharged to the river via surface runoff, soil lateral flow, and groundwater runoff was shown in Figure 9A–C, respectively. The findings showed that each sub-basins' average annual maximum salt loading, which was released into the river by surface runoff, was 0.364 kg/ha·year. The areas with larger discharge intensity were mainly concentrated in the irrigation area of Yigan in the southwestern part of the irrigation area and Jiefangzha. The average annual maximum salt loading discharged into the river through the lateral flow of the soil was 55.6 kg/ha·year, the areas with larger discharge intensity were mainly concentrated in the irrigation area of Yigan in the southwestern part of the irrigation area, and the areas with larger discharge intensity were mainly concentrated in the irrigation area of Yigan in the southwestern part of the irrigation area. The maximum annual salt loading into the river through soil lateral flow was 55.6 kg/ha·year on average, and the areas with higher discharge intensity were mainly concentrated in the Yigan Irrigation Area in the southwestern part of the Irrigation Area, the Jiefangzha Irrigation Area, and the northern part of the sub-basin of the Yi Chang Irrigation Area. On average, the maximum annual salt loading from groundwater runoff to the river was 2454 kg/ha·year, and the areas with higher discharge intensities were concentrated in the Jiefangzha part of the sub-basin in the southwestern part of the irrigation area and in the Yichang and Ulat irrigation areas. This is because the groundwater salinity in the Jiefangzha Irrigation Domain, Yichang Irrigation Domain, and Ulat Irrigation Domain is relatively large, and a large amount of salts are discharged into the river through groundwater runoff, which is conducive to the reduction in groundwater salinity. The intensity of salt discharge loading from each sub-basin in Figure 9A–C also highlights the influence of the strong role of groundwater in the salt loading of surface water.

For each sub-basin, the average annual salt loading from irrigation water and the salt loading that seeps into the shallow aquifer from the soil profile's bottom are depicted in Figure 9D,E, respectively. The areas showing relatively large irrigation water salt loading and seepage salt loading are mainly concentrated in the southwestern part of the irrigation area in the Jiefangzha Irrigation Basin, the northern and east-central part of the Yichang Irrigation Basin, and the northern part of the Ulat Irrigation Basin. This also indicated that the irrigation water volume in these areas was relatively large, and the leaching effect on soil salts was relatively strong, which was conducive to alleviating the intensification of soil salinization. However, the large amount of washed salts entering the groundwater through deep seepage will lead to an increase in the salinity of the groundwater, which may exacerbate the deterioration of the groundwater quality. The salt loading of the aquifer is mainly in the central part of the Jiefangzha irrigation domain, the eastern part of the Yichang irrigation domain, and the Ulat irrigation domain. Therefore, in summary, to control the increase in soil salinity, it is necessary to further improve the drainage engineering measures in these areas. While reducing soil salinity, it can also alleviate the increase in groundwater salinity so that the ecological environment of the HID can be effectively improved.

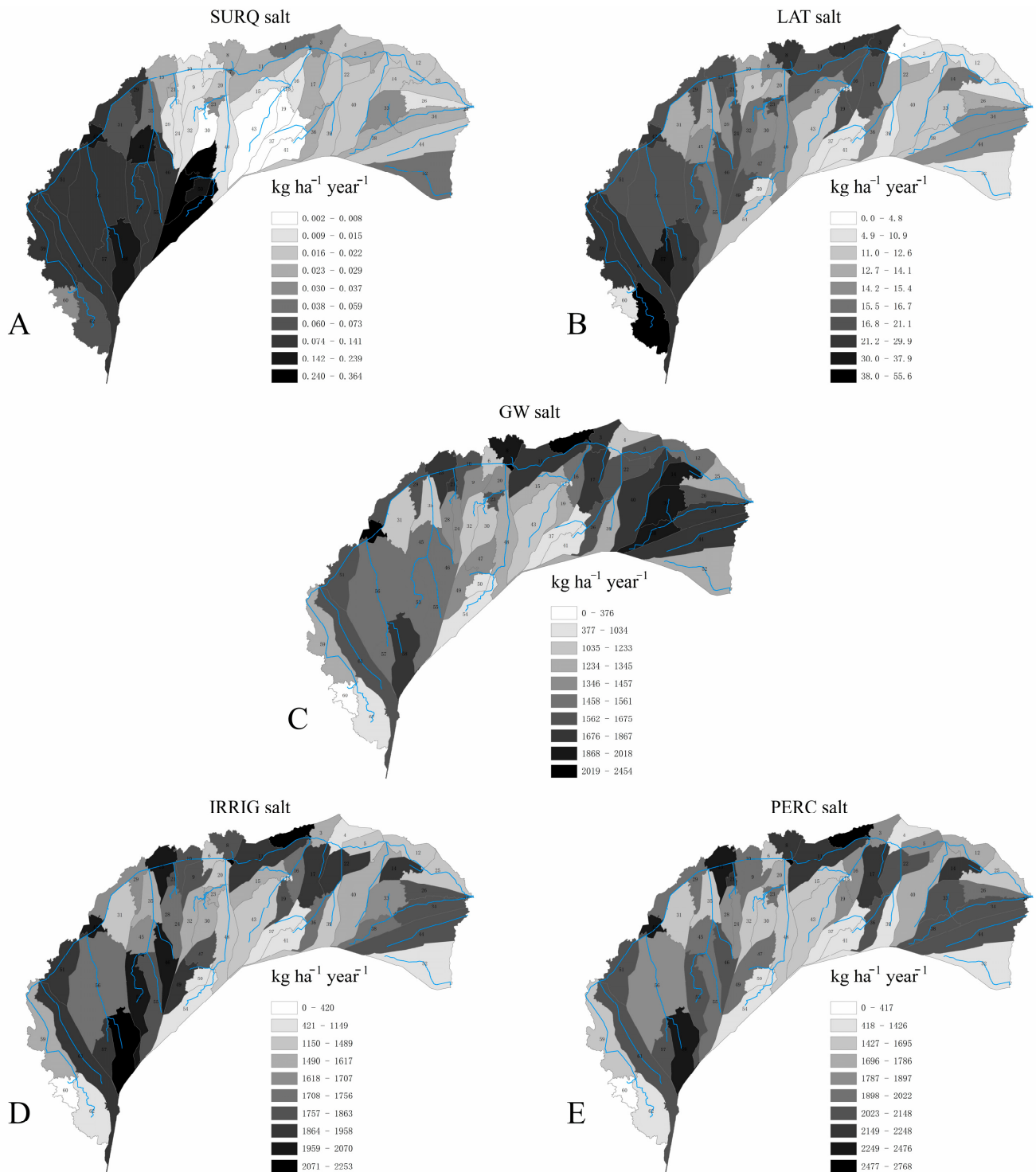


**Figure 9.** The average annual salt loading by sub-basin to (A) surface runoff, (B) lateral flow, (C) groundwater discharge, (D) irrigation water, (E) soil percolation.

### 3.4. Spatial–Temporal Variability of Groundwater and Soil Water Salinity

Based on the monitoring of eight salt ion concentrations and total mineralization in groundwater by 116 groundwater observation wells in the basin from 1996 to 2013 on 6 January, 6 March, 26 May, 16 July, 16 September, 16 October, and 11 November of each year, the model outputs the eight salt ion concentrations of the groundwater in each HRU at that moment in time by the corresponding monitoring time and analyzes them in comparison with the observed values. A comparison of the observed and simulated

values of the average groundwater salinity in the HID between 1996 and 2013 is presented in Figure 10A. The irrigation district's average groundwater salinity was measured to be between 3937.3 and 4724.3 mg/L, while the simulated values were between 4027.3 and 4548.5 mg/L. The simulated values of the other years are generally in good agreement with the observed values, except for the relatively large deviation between the observed and simulated values of average groundwater salinity in 1996 and 1997. Furthermore, the interannual change pattern for both of them indicated a tendency of decreasing, then increasing, and then decreasing. Figure 10B compares the values that were observed and those that were simulated for each of the eight salt ion concentrations in the HID, where the simulated concentration value (187.9 mg/L) is marginally higher than the observed value (148.0 mg/L). The simulated values of  $\text{SO}_4^{2-}$ ,  $\text{Na}^+$ , and  $\text{Cl}^-$  concentrations (715.3 mg/L, 1024.4 mg/L, 1450.6 mg/L) are slightly smaller than the observed values (726 mg/L, 1042.1 mg/L, 1062.2 mg/L), and the remaining ion concentrations have values that are comparable between simulation and observation. Also, the simulated (4278.6 mg/L) and observed (4279.8 mg/L) values of average TDS were similar. The overall results can better reflect the changes in groundwater salinity and different ions in the HID.

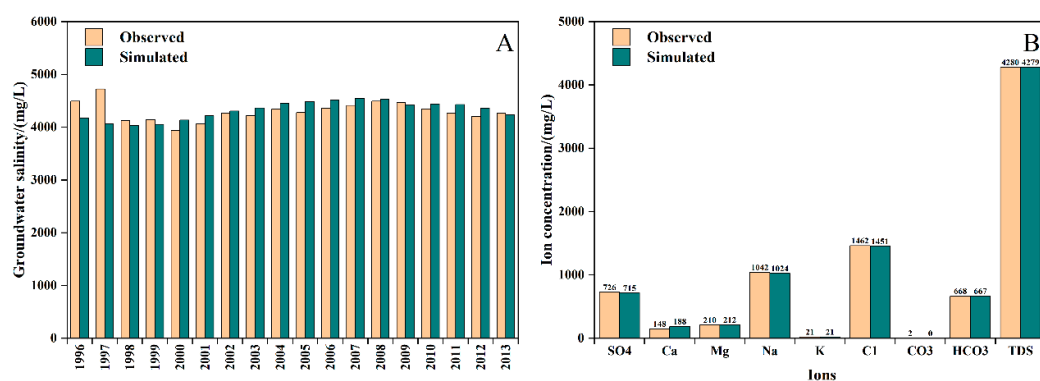


**Figure 10.** Comparison of simulated and measured values of groundwater salinity (A) and eight ion concentrations (B) in the study area.

Figure 11A–E shows the spatial distribution of  $\text{Na}^+$ ,  $\text{Cl}^-$ ,  $\text{SO}_4^{2-}$ ,  $\text{HCO}_3^-$ , and TDS in each HRU from 1996 to 2013, respectively. The distribution of the salts in the groundwater exhibits clear spatial variability, with  $\text{Na}^+$  concentrations between 56 and 5799 mg/L,  $\text{Cl}^-$  concentrations between 117 and 9220 mg/L,  $\text{SO}_4^{2-}$  concentrations between 112 and 5824 mg/L,  $\text{HCO}_3^-$  concentrations between 256 and 1760 mg/L, and TDS concentrations between 822 and 18,713 mg/L. The model underestimates the concentration of  $\text{HCO}_3^-$ . Overall, the eastern part of the basin, i.e., the Yichang and Ulat irrigation basins, has relatively high groundwater salinity. In addition, groundwater salinity is also high in some areas of the Jiefangzha irrigation basin in the southwest of the basin. The salinity in the soil is influenced by both human activities and natural factors, showing a “plug flower” distribution. The average soil water-saturated conductivity in each HRU from 1996 to 2013 is displayed spatially in Figure 11F. The maximum EC was 43.31 dS/m. Soil salinity in the watershed showed a gradual increase from west to east, and its spatial distribution also showed differences. The amount of  $\text{CaSO}_4$  in the aquifer and soil layer after the simulation period is shown in Figure 11G,H. The amount of  $\text{CaSO}_4$  in the soil layer dropped as compared to the start of the simulation. However, the content of  $\text{CaSO}_4$  in the aquifer in the eastern part of the basin increased. This is a side effect of the increasing mineralization of the groundwater in the HID east and the precipitation of salt ions into corresponding salt minerals.

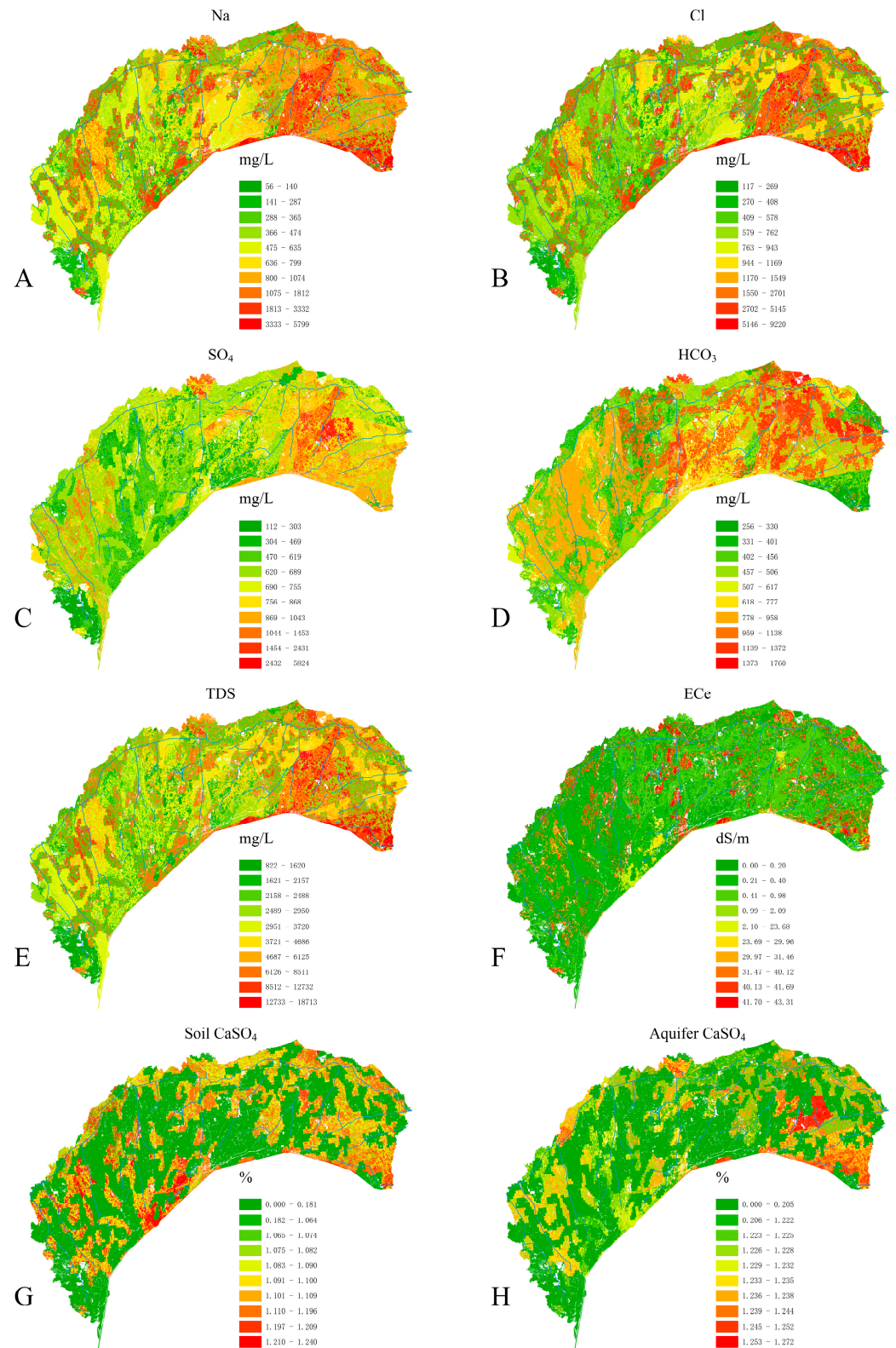


**Figure 11.** Average groundwater salinity (Na (A), Cl (B), SO<sub>4</sub> (C), HCO<sub>3</sub> (D), TDS (E), Soil CaSO<sub>4</sub> (G) and Aquifer CaSO<sub>4</sub> (H) and average soil water electrical conductivity (F) in HRU from 1998 to 2007.

### 3.5. Changes in Water Salinity for Different Land Uses and Soil Types

Groundwater salinity and EC for various land-use types (A) and soil types (B) are shown in Figure 12. Among the land-use types include Cropland (AGRR), Spring Wheat (SWHT), Corn (CORN), Sunflower (SUNF), Watershed (WATR), Bare Ground (BARR),

Forest (FRST), and Town (BERM). Soil types include Cambic Arenosols (Arb), Haplic Arenosols (ARh), Cumulic Anthrosols (ATc), Calcaric Fluvisols (FLc), Mollic Gleysols (GLm), SCm, and Water bodies (WR). Their results showed that the average groundwater salinity (2946 mg/L) and EC (0.309 dS/m) were less in AGRR compared to BARR, FRST, and BERM. In particular, the average groundwater salinity of BERM reached 8605 mg/L, and the EC of BARR reached 18.975 dS/m. Among the different planting crops, the average groundwater salinity (2464 mg/L) and EC (0.282 dS/m) of SWHT were smaller compared to the other three crops. Therefore, the optimization of cropping structures can be considered to reduce the salt content in groundwater and soil appropriately. A comparison of different soil types shows that groundwater salinity (5015 mg/L) and EC (13.18 dS/m) are larger in SCm. This also laterally reflects that the soil with high salt content has a greater influence on the water salinity changes in the HID. In addition, combining Figure 12A,B, it can be seen that the lakes in the HID are the main salt sinks for groundwater.

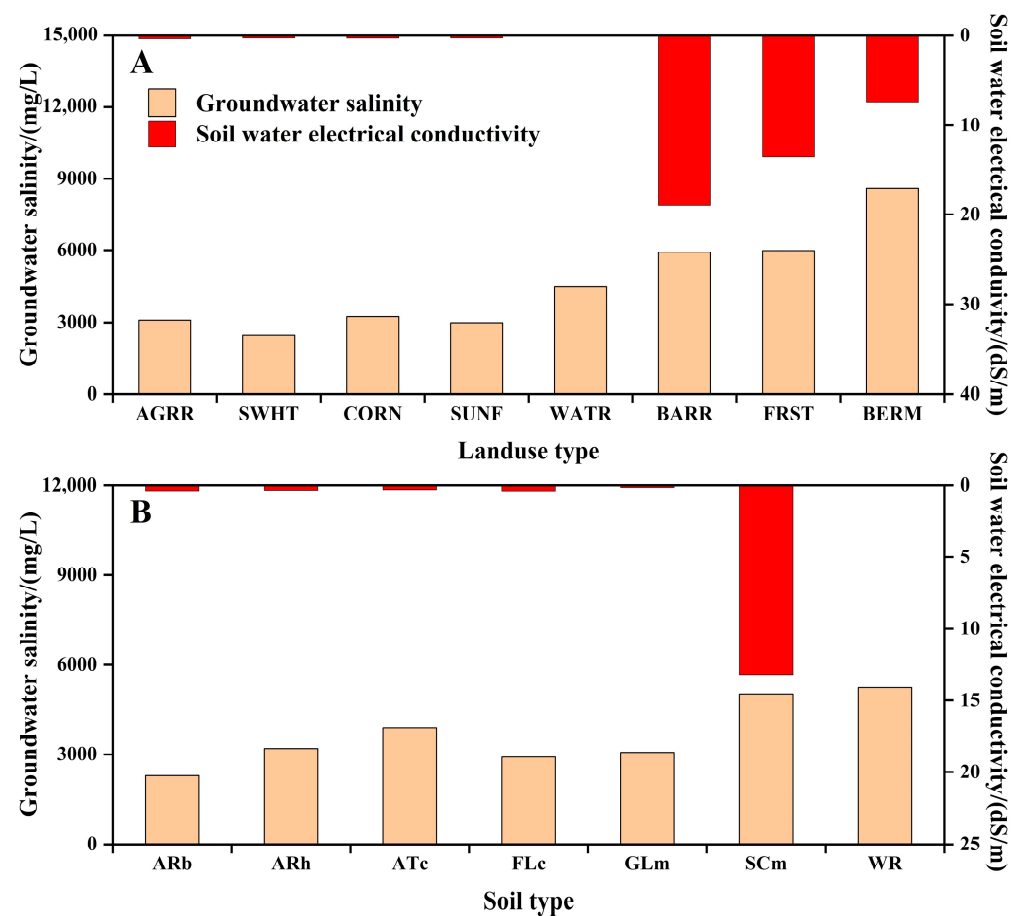


**Figure 12.** Average groundwater salinity and average soil water electrical conductivity in different land uses (A) and soil types (B).

### 3.6. Situational Analysis

It is important to study the changes in water salinity in irrigation districts at the watershed scale with different degrees of water conservation during the fertility and fall watering periods based on the SWAT model fertility and fall watering periods under the existing irrigation water conditions. As shown in Figure 13a, the annual salt discharge load when total irrigation is reduced by 5% (Scenario 1) and irrigation is reduced by 10% during the fall watering period (Scenario 1.2) is greater than when irrigation is reduced by 5% during both the reproductive and fall watering periods (Scenario 1.1); When total irrigation is reduced by 10% (Scenario 2) and total irrigation is reduced by 15% (Scenario 3), the amount of salt discharge loading from reducing the same proportion of irrigation during

the fertility and fall watering periods is greater than the amount of salt discharge loading from reducing different proportions of irrigation during the two periods, and for every 5% reduction in total irrigation, the total salt discharge loading will be reduced by about 13% to 14%. As shown in Figure 13b, salt discharge through groundwater is mainly carried out in the HID, and the reduction in total irrigation volume will lead to the reduction of salt discharge, whereas the salt loading discharged through groundwater is correspondingly reduced accordingly. This also leads to greater groundwater mineralization, and the more the irrigation volume is reduced, the more the groundwater mineralization will increase. Therefore, under the premise of reducing the total irrigation volume, a reasonable allocation of irrigation water at different periods during the year can appropriately increase the amount of salt discharge loading and reduce the groundwater salinity in the HID.

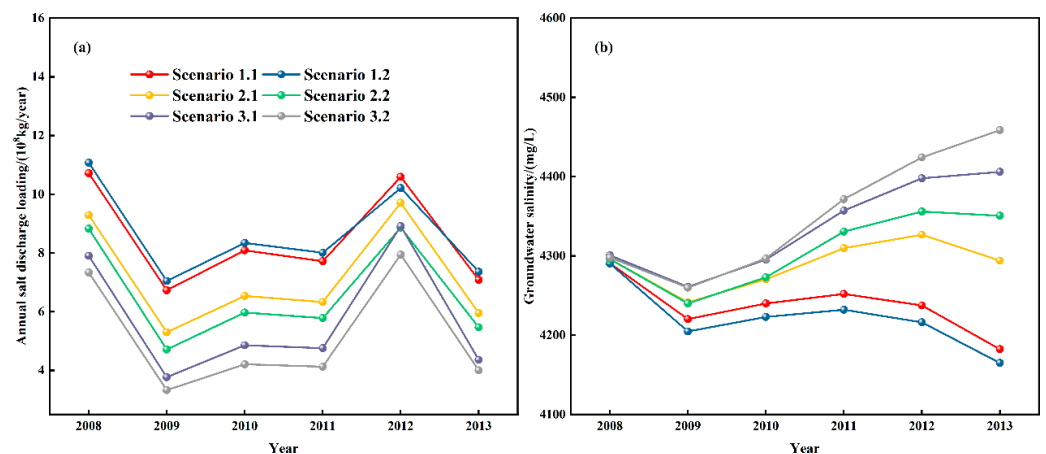


**Figure 13.** Annual salt discharge loading (a) and average Groundwater salinity (b) in different scenarios from 2008 to 2013.

## 4. Discussion

### 4.1. Model Performance

Through validation and calibration, the improved SWAT-Salt module can comprehensively consider the time-series changes and spatial differences in the distribution of drainage discharge salt, groundwater salt, and soil water salt in the HID. However, the magnitude of the concentration of the eight ions in the daily diversion irrigation water was not monitored due to the limited actual observation data. In this study, the same irrigation water ion concentration data during the year were used for generalization. If the concentration magnitude of the eight salt ions in daily diversion irrigation water can be obtained, the trend of irrigation water on soil profile salt loading can be more accurately simulated and analyzed. Furthermore, based on the ion concentration changes in the Yellow River water over an extended period, it is possible to predict and analyze the changes in water salt in the HID in the future when the salt ion composition of the irrigation water changes. Second, the effects of irrigation with brackish water on the soil environment in the HID have already been studied by academics [27,46–48], which can alleviate the risk of the secondary salinization of the soil to a certain extent. Accordingly, the SWAT-Salt model can consider the spatial distribution of saline water in the HID, the amount of extracted water, water quality, and other factors to further explore the impact of combined saline and freshwater irrigation on salt recharge and drainage balance in the HID at the watershed scale.

The primary applications of SWAT are in irrigation water basins, where segments of natural rivers are intercepted and fed into the model, and in natural watersheds, where rivers typically have their source in mountain ranges. Water redirected from outside the basin is the primary source of irrigation for the HID; however, the salinity from irrigation sources outside the basin is not captured by the SWAT-Salt model. The simulated annual salt discharge loading at the basin outlet is  $73.9 \times 10^8$  kg, 73.9% less than the actual value if

salts are ignored in the model (see Figure 5). However, after modification, the error was only 3.9% different. To sum up, the SWAT-Salt model provides a more accurate description of the water and salt transport mechanism in the HID.

#### 4.2. Characterization of Water Salinity in the HID

Water from the Yellow River is primarily diverted to provide irrigation water for the HID throughout its life cycle. Nevertheless, it will subsequently increase the soil salinity content. This causes the amount of salt diversion and discharge during the reproductive and fall watering periods to increase accordingly. Therefore, how to appropriately distribute irrigation water during the reproductive period and the amount of fall watering plays a crucial role in the normal growth of crops as well as salt washing and salt suppression in fall watering [49].

The trend of monthly salt discharge loading in the HID was the same as that of runoff, which was mainly concentrated in the reproductive period and fall watering period. Among them, the drainage salt loading during the reproductive period and fall watering period accounted for 35.8% and 55.4% of the annual drainage salt loading, respectively. This is because drainage salt loading during the reproductive period is comparatively low in Inner Mongolia. After all, drip irrigation is mostly utilized during this time. Nonetheless, the primary purpose of the fall watering season is to soak the soil water salts with greater amounts of diffuse irrigation, which causes more drainage and salt exclusion during this time. This also indicates that the fall watering period has a better effect on soil salt exclusion [50]. The hydrological runoff in the HID mainly consists of surface runoff, soil lateral flow, and groundwater runoff. Although the HID has a relatively flat topography, groundwater processes primarily handle drainage and salt exclusion, with relatively little surface runoff and soil lateral flow, whereas, among the different hydrological pathways, the salt discharge loading from groundwater accounted for about 98.7% or so of the total salt discharge loading from each hydrological pathway, which was the main contributing part of salt discharge in the HID. This emphasizes how important groundwater salt discharge is to the HID's salt discharge. Furthermore, 55.6 kg/ha-year was the highest average annual salt loading that was released into the river by soil lateral flow. Moreover, the areas with higher discharge intensity were mainly concentrated in the Yigan irrigation domain, Jiefangzha irrigation domain, and some sub-basins in the northern part of the Yichang irrigation domain in the southwestern part of the HID. This is due to the influence of topography. The HID's northern and southwestern sections have higher topographic slopes and are comparatively higher than the district's central and eastern regions. It results in relatively large salt loadings discharged into the river from surface runoff and lateral flow in the sub-watersheds in which these regions are located [51–53].

The sustainable growth of agriculture in irrigation areas is significantly impacted by soil salinization. To address the salinization issue, researchers have done a great deal of study. One option is to switch out the conventional diffuse irrigation with more efficient and water-saving technology. This delivers water more precisely to the plant roots, reduces water wastage, and improves irrigation efficiency, thus saving water and costs. It also reduces water and fertilizer runoff, thus reducing environmental pollution. The main point is to prevent the rapid rise of the water table from returning salt to the soil layer while at the same time achieving water savings and reducing the risk of salinization [54,55]. On the other hand, the technology of concealed pipe drainage and salt removal can be promoted to prevent the problem of salt return by the evaporation of soil moisture, which can effectively improve the problem of soil salinization in Inner Mongolia. Meanwhile, it has been obtained in the related studies of scholars that culvert pipe drainage and salt removal technology can effectively reduce the soil salt content [56–58]. However, since the culvert pipe needs to drain water from the soil to the alkali drainage canal, it may lead to an increase in salt loading downstream. Therefore, the synergy of rational irrigation system and engineering measures plays an important role in improving the soil salinity problem in Inner Mongolia.

#### 4.3. Model Applications and Limitations

As of now, besides the Inner Mongolia region, there are still very many saline irrigated areas in the world, but there is no suitable tool to analyze and study the regional water and salt transport patterns, whereas the improved SWAT-Salt model can perfect the salt deficiency in the irrigation setup. This renders it applicable to both irrigation water sources from groundwater areas and canals inside the watershed as well as those from groundwater areas and canals outside of it. The improved SWAT-Salt model provides an analytical tool for developing salinity control programs in this study.

However, the SWAT model itself has some limitations. First, the model studies the hydrological material cycle in each HRU separately, while the HRUs are independent of each other and have no spatial connection. Moreover, the transfer of salt and water between distinct HRUs cannot be taken into consideration [59]. Second, when it comes to simulating the movement of water and salt in groundwater and soil water, the SWAT model is not based on physical groundwater dynamics, the Richards equation for soil water, or solute transport laws. Therefore, the model may be inaccurate [30,33,60] for changes in salt transport in groundwater and soil water (as shown in Section 3.3). As mentioned by Bailey et al. [33], MODFLOW has been widely used for groundwater flow movement processes. The SWAT-MODFLOW-Salt model, which can more accurately simulate the process of salt transport in groundwater, can be created by integrating the salt module into the SWAT-MODFLOW [46]. Moreover, we will actively carry out the research on this part in subsequent studies.

#### 5. Conclusions

The improved SWAT-Salt model applied to the HID served as the foundation for the construction of a distributed water and salt transport model for arid and semi-arid agricultural irrigation basins in this study. Through the model calibration and validation, the model can comprehensively consider the spatial–temporal distribution characteristics and transport laws of drainage salt, groundwater salt, and soil water salt in the HID. The main conclusions are as follows:

- (1) Based on comparisons of impacts before and after model modification as well as evaluation indexes of monthly salt discharge loading and streamflow simulated by the model, the distributed salt and water transport model SWAT-Salt can more accurately simulate the water and salt transport pattern of HID.
- (2) The trend of monthly salt discharge loading in the HID was consistent with that of streamflow, which was mainly concentrated in the fertility period and the autumn watering period, in which the salt discharge loading in the fertility period and the autumn watering period accounted for 35.8% and 55.4% of the annual salt discharge loading, respectively. Among the different hydrological paths, the salt discharge loading of groundwater accounted for about 98.7% of the total salt discharge loading of the hydrological paths.
- (3) In the spatial distribution pattern of water and salt in the HID, the salt loading of surface runoff and lateral flow is mainly concentrated in the southwestern part of the basin, and the salt discharge loading of groundwater is mainly concentrated in the eastern part of the basin as well as some sub-basins in the southwestern part of the basin.
- (4) Groundwater salinity and EC in the HID show large spatial variability. Groundwater salinity is larger in the Yichang and Ulat irrigation domains in the eastern part of the HID, and groundwater salinity is also relatively larger in some areas of the Jiefangzha irrigation domain in the east. From west to east, the overall EC for the salt concentration in the soil progressively grows, as does the salt content of the soil.
- (5) Groundwater salinity and EC of cropland in the HID was smaller compared to other land-use types, and wheat had the lowest average groundwater salinity (2464 mg/L) and EC (0.282 dS/m).

- (6) Under the premise of reducing the total irrigation volume, a reasonable allocation of irrigation water at different periods during the year can appropriately increase the amount of salt discharge loading and reduce the salinity of groundwater in the HID.

The SWAT-Salt model has certain inherent flaws that make it unable to accurately predict the groundwater movement process when compared to other field-scale or regional-scale water and salt models. However, with the great advantage of distributed hydrological modeling, it can better reflect the spatial–temporal distribution differences of water salinity at the scale of a long series of basins. In this way, different irrigation methods and saline–alkaline land improvement measures can be adopted to improve the farmland ecological environment in the HID and reduce the harm of salinity on crop growth, water quality deterioration, and soil salinization. It can serve as a guide for the irrigation area’s stable and sustainable development.

**Author Contributions:** Conceptualization, C.A. and J.D.; methodology, D.J. and R.T.B.; software, W.Z.; validation, C.A., J.D. and J.H.; formal analysis, D.J. and J.D.; investigation, R.T.B., W.Z. and J.H.; data curation, C.A. and J.D.; writing—original draft preparation, C.A.; writing—review and editing, J.D. and J.H.; visualization, D.J., R.T.B. and J.D.; funding acquisition, C.A., W.Z. and J.H. All authors have read and agreed to the published version of the manuscript.

**Funding:** This study was funded by the National Key Research and Development Program of China (Grant No. 2021YFD1900805-03), the National Natural Science Foundation of China (NSFC) (Grant Nos. 52179039 and 52009093), and the Fundamental Research Funds for the Central Universities (Grant No. 2042023kf0158).

**Data Availability Statement:** The datasets in this study are available from the corresponding author upon reasonable request.

**Conflicts of Interest:** The authors declare no conflicts of interest.

## References

- Jacobsen, T.; Adams, R.M. Salt and Silt in Ancient Mesopotamian Agriculture: Progressive changes in soil salinity and sedimentation contributed to the breakup of past civilizations. *Science* **1958**, *128*, 1251–1258. [[CrossRef](#)] [[PubMed](#)]
- Cuevas, J.; Daliakopoulos, I.N.; Del Moral, F.; Hueso, J.J.; Tsanis, I.K. A review of soil-improving cropping systems for soil salinization. *Agronomy* **2019**, *9*, 295. [[CrossRef](#)]
- Singh, A. Soil salinization management for sustainable development: A review. *J. Environ. Manag.* **2021**, *277*, 111383. [[CrossRef](#)] [[PubMed](#)]
- Cao, Z.; Zhu, T.; Cai, X. Hydro-agro-economic optimization for irrigated farming in an arid region: The Hetao Irrigation District, Inner Mongolia. *Agric. Water Manag.* **2023**, *277*, 108095. [[CrossRef](#)]
- Chang, X.; Gao, Z.; Wang, S.; Chen, H. Modelling long-term soil salinity dynamics using SaltMod in Hetao Irrigation District, China. *Comput. Electron. Agric.* **2019**, *156*, 447–458. [[CrossRef](#)]
- Wu, M.; Huang, J.; Tan, X.; Wu, J. Water, salt and heat influences on carbon and nitrogen dynamics in seasonally frozen soils in Hetao Irrigation District, Inner Mongolia, China. *Pedosphere* **2019**, *29*, 632–641. [[CrossRef](#)]
- Ramos, T.B.; Liu, M.; Paredes, P.; Shi, H.; Feng, Z.; Lei, H.; Pereira, L.S. Salts dynamics in maize irrigation in the Hetao plateau using static water table lysimeters and HYDRUS-1D with focus on the autumn leaching irrigation. *Agric. Water Manag.* **2023**, *283*, 108306. [[CrossRef](#)]
- Dou, X.; Shi, H.; Li, R.; Miao, Q.; Yan, J.; Tian, F.; Wang, B. Simulation and evaluation of soil water and salt transport under controlled subsurface drainage using HYDRUS-2D model. *Agric. Water Manag.* **2022**, *273*, 107899. [[CrossRef](#)]
- Lu, X.; Li, R.; Shi, H.; Liang, J.; Miao, Q.; Fan, L. Successive simulations of soil water-heat-salt transport in one whole year of agriculture after different mulching treatments and autumn irrigation. *Geoderma* **2019**, *344*, 99–107. [[CrossRef](#)]
- Yuan, C. Simulation soil water–salt dynamics in saline wasteland of Yongji Irrigation Area in Hetao Irrigation District of China. *Water Supply* **2021**, *21*, 2681–2690. [[CrossRef](#)]
- Mao, W.; Yang, J.; Zhu, Y.; Ye, M.; Wu, J. Loosely coupled SaltMod for simulating groundwater and salt dynamics under well-canal conjunctive irrigation in semi-arid areas. *Agric. Water Manag.* **2017**, *192*, 209–220. [[CrossRef](#)]
- Xie, W.; Yang, J.; Yao, R.; Wang, X. Spatial and temporal variability of soil salinity in the Yangtze River estuary using electromagnetic induction. *Remote Sens.* **2021**, *13*, 1875. [[CrossRef](#)]
- Li, H.; Liu, X.; Hu, B.; Biswas, A.; Jiang, Q.; Liu, W.; Wang, N.; Peng, J. Field-scale characterization of spatio-temporal variability of soil salinity in three dimensions. *Remote Sens.* **2020**, *12*, 4043. [[CrossRef](#)]
- Hu, Z.; Miao, Q.; Shi, H.; Feng, W.; Hou, C.; Yu, C.; Mu, Y. Spatial Variations and Distribution Patterns of Soil Salinity at the Canal Scale in the Hetao Irrigation District. *Water* **2023**, *15*, 3342. [[CrossRef](#)]

15. Huang, Q.; Xu, X.; Lü, L.; Ren, D.; Ke, J.; Xiong, Y.; Huo, Z.; Huang, G. Soil salinity distribution based on remote sensing and its effect on crop growth in Hetao Irrigation District. *Trans. Chin. Soc. Agric. Eng.* **2018**, *34*, 102–109.
16. Hao, Y.; Xu, X.; Ren, D.; Huang, Q.; Huang, G. Distributed modeling of soil water-salt dynamics and crop yields based on HYDRUS-EPIC model in Hetao Irrigation District. *Trans. Chin. Soc. Agric. Eng.* **2015**, *31*, 110–116.
17. Xu, X.; Huang, G.; Zhan, H.; Qu, Z.; Huang, Q. Integration of SWAP and MODFLOW-2000 for modeling groundwater dynamics in shallow water table areas. *J. Hydrol.* **2012**, *412*, 170–181. [[CrossRef](#)]
18. Xiong, L.; Xu, X.; Ren, D.; Huang, Q.; Huang, G. Enhancing the capability of hydrological models to simulate the regional agro-hydrological processes in watersheds with shallow groundwater: Based on the SWAT framework. *J. Hydrol.* **2019**, *572*, 1–16. [[CrossRef](#)]
19. Wang, R.; Xiong, L.; Xu, X.; Liu, S.; Feng, Z.; Wang, S.; Huang, Q.; Huang, G. Long-term responses of the water cycle to climate variability and human activities in a large arid irrigation district with shallow groundwater: Insights from agro-hydrological modeling. *J. Hydrol.* **2023**, *626*, 130264. [[CrossRef](#)]
20. Liu, Y.; Li, F.; Zhao, Y. Improved hydrological modelling and ET estimation in watershed with irrigation interference. *J. Hydrol.* **2024**, *634*, 131108. [[CrossRef](#)]
21. Guermoui, M.; Melgani, F.; Gairaa, K.; Mekhalfi, M.L. A comprehensive review of hybrid models for solar radiation forecasting. *J. Clean. Prod.* **2020**, *258*, 120357. [[CrossRef](#)]
22. Tung, T.M.; Yaseen, Z.M. A survey on river water quality modelling using artificial intelligence models: 2000–2020. *J. Hydrol.* **2020**, *585*, 124670.
23. Stavi, I.; Thevs, N.; Priori, S. Soil salinity and sodicity in drylands: A review of causes, effects, monitoring, and restoration measures. *Front. Environ. Sci.* **2021**, *9*, 712831. [[CrossRef](#)]
24. Daba, A.W.; Qureshi, A.S. Review of soil salinity and sodicity challenges to crop production in the lowland irrigated areas of Ethiopia and its management strategies. *Land* **2021**, *10*, 1377. [[CrossRef](#)]
25. Yang, Y.; Zhu, Y.; Mao, W.; Dai, H.; Ye, M.; Wu, J.; Yang, J. Study on the Exploitation Scheme of Groundwater under Well-Canal Conjunctive Irrigation in Seasonally Freezing-Thawing Agricultural Areas. *Water* **2021**, *13*, 1384. [[CrossRef](#)]
26. Zhang, X.; Guo, P.; Zhang, F.; Liu, X.; Yue, Q.; Wang, Y. Optimal irrigation water allocation in Hetao Irrigation District considering decision makers' preference under uncertainties. *Agric. Water Manag.* **2021**, *246*, 106670. [[CrossRef](#)]
27. Guo, K.; Liu, X. Reclamation effect of freezing saline water irrigation on heavy saline-alkali soil in the Hetao Irrigation District of North China. *Catena* **2021**, *204*, 105420. [[CrossRef](#)]
28. Arnold, J.G.; Srinivasan, R.; Muttiah, R.S.; Williams, J.R. Large area hydrologic modeling and assessment part I: Model development. *J. Am. Water Resour. Assoc.* **1998**, *34*, 73–89. [[CrossRef](#)]
29. Srinivasan, R.; Ramanarayanan, T.S.; Arnold, J.G.; Bednarz, S.T. Large area hydrologic modeling and assessment part II: Model application. *J. Am. Water Resour. Assoc.* **1998**, *34*, 91–101. [[CrossRef](#)]
30. Neitsch, S.L.; Arnold, J.G.; Kiniry, J.R.; Williams, J.R. *Soil and Water Assessment Tool Theoretical Documentation Version 2009*; Texas Water Resources Institute: College Station, TX, USA, 2011.
31. Hussain, M.I.; Farooq, M.; Muscolo, A.; Rehman, A. Crop diversification and saline water irrigation as potential strategies to save freshwater resources and reclamation of marginal soils—A review. *Environ. Sci. Pollut. Res.* **2020**, *27*, 28695–28729. [[CrossRef](#)]
32. Tedeschi, A. Irrigated agriculture on saline soils: A perspective. *Agronomy* **2020**, *10*, 1630. [[CrossRef](#)]
33. Bailey, R.T.; Tavakoli-Kivi, S.; Wei, X. A salinity module for SWAT to simulate salt ion fate and transport at the watershed scale. *Hydrol. Earth Syst. Sci.* **2019**, *23*, 3155–3174. [[CrossRef](#)]
34. Jiang, D.; Ao, C.; Bailey, R.T.; Zeng, W.; Huang, J. Simulation of water and salt transport in the Kaidu River Irrigation District using the modified SWAT-Salt. *Agric. Water Manag.* **2022**, *272*, 107845. [[CrossRef](#)]
35. Winchell, M.; Srinivasan, R.; Di Luzio, M.; Arnold, J. *ArcSWAT Interface for SWAT2012: User's Guide*; Blackland Research Center, Texas AgriLife Research: College Station, TX, USA, 2013; pp. 1–464.
36. Caldeira, T.L.; Mello, C.R.; Beskow, S.; Timm, L.C.; Viola, M.R. LASH hydrological model: An analysis focused on spatial discretization. *Catena* **2019**, *173*, 183–193. [[CrossRef](#)]
37. Martz, L.W.; Garbrecht, J. The treatment of flat areas and depressions in automated drainage analysis of raster digital elevation models. *Hydrol. Process.* **1998**, *12*, 843–855. [[CrossRef](#)]
38. Saunders, W.K.; Maidment, D.R. *A GIS Assessment of Nonpoint Source Pollution in the San Antonio-Nueces Coastal Basin*; Center for Research in Water Resources, University of Texas at Austin: Austin, TX, USA, 1996.
39. FAO; ISRIC. *Harmonized World Soil Database (Version 1.2)*; FAO: Rome, Italy; IIASA: Laxenburg, Austria, 2012.
40. Abbaspour, K.C. *SWAT Calibration and Uncertainty Programs—A User Manual*; Swiss Federal Institute of Aquatic Science and Technology: Duebendorf, Switzerland, 2015; Volume 103, pp. 17–66.
41. Dong, J.; Zeng, W.; Lei, G.; Wu, L.; Chen, H.; Wu, J.; Huang, J.; Gaiser, T.; Srivastava, A.K. Simulation of dew point temperature in different time scales based on grasshopper algorithm optimized extreme gradient boosting. *J. Hydrol.* **2022**, *606*, 127452. [[CrossRef](#)]
42. Dong, J.; Zeng, W.; Wu, L.; Huang, J.; Gaiser, T.; Srivastava, A.K. Enhancing short-term forecasting of daily precipitation using numerical weather prediction bias correcting with XGBoost in different regions of China. *Eng. Appl. Artif. Intell.* **2023**, *117*, 105579. [[CrossRef](#)]

43. Tavakkoli, E.; Rengasamy, P.; McDonald, G.K. High concentrations of Na<sup>+</sup> and Cl<sup>-</sup> ions in soil solution have simultaneous detrimental effects on growth of faba bean under salinity stress. *J. Exp. Bot.* **2010**, *61*, 4449–4459. [[CrossRef](#)]
44. Zhang, S.; Han, G.; Zeng, J.; Xiao, X.; Malem, F. A strontium and hydro-geochemical perspective on human impacted tributary of the Mekong River Basin: Sources identification, fluxes, and CO<sub>2</sub> consumption. *Water* **2021**, *13*, 3137. [[CrossRef](#)]
45. Chen, Y.; Matsui, Y.; Sato, T.; Shirasaki, N.; Matsushita, T. Overlooked effect of ordinary inorganic ions on polyaluminum-chloride coagulation treatment. *Water Res.* **2023**, *235*, 119909. [[CrossRef](#)]
46. Bailey, R.T.; Wible, T.C.; Arabi, M.; Records, R.M.; Ditty, J. Assessing regional-scale spatio-temporal patterns of groundwater-surface water interactions using a coupled SWAT-MODFLOW model. *Hydrol. Process.* **2016**, *30*, 4420–4433. [[CrossRef](#)]
47. Wang, R.; Huang, G.; Xu, X.; Ren, D.; Gou, J.; Wu, Z. Significant differences in agro-hydrological processes and water productivity between canal-and well-irrigated areas in an arid region. *Agric. Water Manag.* **2022**, *267*, 107637. [[CrossRef](#)]
48. Hou, C.; Miao, Q.; Shi, H.; Hu, Z.; Zhao, Y.; Yu, C.; Yan, Y.; Feng, W. Water and Salinity Variation along the Soil Profile and Groundwater Dynamics of a Fallow Cropland System in the Hetao Irrigation District, China. *Water* **2023**, *15*, 4098. [[CrossRef](#)]
49. Abd El-Mageed, T.A.; Semida, W.M.; Abd El-Wahed, M.H. Effect of mulching on plant water status, soil salinity and yield of squash under summer-fall deficit irrigation in salt affected soil. *Agric. Water Manag.* **2016**, *173*, 1–12. [[CrossRef](#)]
50. Zheng, N.; Guo, M.; Yue, W.; Teng, Y.; Zhai, Y.; Yang, J.; Zuo, R. Evaluating the impact of flood irrigation on spatial variabilities of soil salinity and groundwater quality in an arid irrigated region. *Hydrol. Res.* **2021**, *52*, 229–240. [[CrossRef](#)]
51. Brunner, P.A. Water and salt management in the Yanqi Basin, China. Ph.D. Thesis, ETH Zurich, Valendas, Switzerland, 2005.
52. Li, J.; Luo, Q.; Dong, M.; Nie, G.; Liu, Z.; Wu, Z. Synthesis of granulated Li/Al-LDHs adsorbent and application for recovery of Li from synthetic and real salt lake brines. *Hydrometallurgy* **2022**, *209*, 105828. [[CrossRef](#)]
53. An, D.; Zhao, G.; Chang, C.; Wang, Z.; Li, P.; Zhang, T.; Jia, J. Hyperspectral field estimation and remote-sensing inversion of salt content in coastal saline soils of the Yellow River Delta. *Int. J. Remote Sens.* **2016**, *37*, 455–470. [[CrossRef](#)]
54. Karimov, A.K.; Šimůnek, J.; Hanjra, M.A.; Avliyakov, M.; Forkutsa, I. Effects of the shallow water table on water use of winter wheat and ecosystem health: Implications for unlocking the potential of groundwater in the Fergana Valley (Central Asia). *Agric. Water Manag.* **2014**, *131*, 57–69. [[CrossRef](#)]
55. Fu, X.; Wu, X.; Wang, H.; Chen, Y.; Wang, R.; Wang, Y. Effects of fertigation with carboxymethyl cellulose potassium on water conservation, salt suppression, and maize growth in salt-affected soil. *Agric. Water Manag.* **2023**, *287*, 108436. [[CrossRef](#)]
56. Heng, T.; Liao, R.; Wang, Z.; Wu, W.; Li, W.; Zhang, J. Effects of combined drip irrigation and sub-surface pipe drainage on water and salt transport of saline-alkali soil in Xinjiang, China. *J. Arid Land.* **2018**, *10*, 932–945. [[CrossRef](#)]
57. Liu, Y.; Ao, C.; Zeng, W.; Srivastava, A.K.; Gaiser, T.; Wu, J.; Huang, J. Simulating water and salt transport in subsurface pipe drainage systems with HYDRUS-2D. *J. Hydrol.* **2021**, *592*, 125823. [[CrossRef](#)]
58. Qian, Y.; Zhu, Y.; Ye, M.; Huang, J.; Wu, J. Experiment and numerical simulation for designing layout parameters of subsurface drainage pipes in arid agricultural areas. *Agric. Water Manag.* **2021**, *243*, 106455. [[CrossRef](#)]
59. Mu, D.; Xun, Y.; Gao, Y.; Ren, D.; Sun, C.; Ma, X.; Huang, G.; Xu, X. A modified SWAT model for mechanistic simulation of soil water-salt transport and the interactions with shallow groundwater. *Hydrol. Process.* **2023**, *37*, e14980. [[CrossRef](#)]
60. Tirabadi, M.S.M.; Banihabib, M.E.; Randhir, T.O. SWAT-S: A SWAT-salinity module for watershed-scale modeling of natural salinity. *Environ. Modell. Softw.* **2021**, *135*, 104906. [[CrossRef](#)]

**Disclaimer/Publisher’s Note:** The statements, opinions and data contained in all publications are solely those of the individual author(s) and contributor(s) and not of MDPI and/or the editor(s). MDPI and/or the editor(s) disclaim responsibility for any injury to people or property resulting from any ideas, methods, instructions or products referred to in the content.